JAERI-M
83-140

EVALUATION REPORT ON CCTF CORE-I REFLOOD TEST C1-1 (RUN 010)

—INVESTIGATION OF THE LOOP FLOW RESISTANCE EFFECT—

September 1983

Takashi SUDOH* and Yoshio MURAO

日本原子力研究所
Japan Atomic Energy Research Institute

JAERI-M レポートは，日本原子力研究所が不定期に公刊している研究報告書です。
入手の問合わせは，日本原子力研究所技術情報部情報資料課（〒319—11 茨城県那珂郡東海村）あて，お申しこしください。なお，このほかに財団法人原子力弘済会資料センター（〒319-11 茨城県那珂郡東海村日本原子力研究所内）で複写による実費頒布をおこなっております。

JAERI-M reports are issued irregularly.
Inquiries about availability of the reports should be addressed to Information Section, Division of Technical Information, Japan Atomic Energy Research Institute, Tokai-mura, Naka-gun, Ibaraki-ken 319-11, Japan.

編集兼発行　日本原子力研究所
印　　刷　山田軽印刷所

JAERI-M 83-140

EVALUATION REPORT ON CCTF CORE-I REFLOOD TEST C1-1 (RUN 010)

—— Investigation of the loop flow resistance effect ——

Takashi SUDOH* and Yoshio MURAO

Department of Nuclear Safety Research,

Tokai Research Establishment, JAERI

(Received August 9, 1983)

This report describes the effects of the loop flow resistance on the thermohydraulic behavior in the primary system during the reflood phase. The investigation is based on the results of the test C1-1 which was performed with increased loop flow resistance in the Cylindrical Core Test Facility (CCTF) at Japan Atomic Energy Research Institute.

The loop flow resistance was about 40% higher in the present test than in the reference test C1-5. The results of two tests were compared and the following conclusions were obtained:

1) The total loop flow rate and the core flooding rate were reduced by about 20% with the increased loop flow resistance
2) The core heat transfer was also lowered, then, the turnaround and the quench times extended at the locations above the core midplane.
3) The measured maximum temperature in the core was 50 K higher for the present test than for the reference test.

Keywords: PWR, LOCA, ECCS, REFLOOD, Heat-transfer, Loop-Flow-registance, Quench, Turnaround

---

The work was performed under contract with the Atomic Energy Bureau of Science and Technology Agency of Japan.

* Nuclear Data Center

大型再冠水円筒第1次炉心試験C1-1（RUN 010）評価報告書
—— 再冠水挙動に及ぼすループ流動抵抗の効果 ——

日本原子力研究所東海研究所安全工学部
須藤　高史*・村尾　良夫

（1983年8月9日受理）

本報告書は，日本原子力研究所の円筒炉心試験装置で行なわれた試験の中でループ流動抵抗を増大させた試験に注目し，再冠水期における，ループ流動抵抗の熱水力挙動に及ぼす影響について述べたものである。

本試験は，基準試験より約40％ループ流動抵抗を増大させて行なわれた。本試験及び基準試験の結果の比較を行い，次のような結論を得た。

(1) 40％のループ流動抵抗増大により，ループ蒸気流量は約20％減少し，また，冠水速度も同様に20％減少した。

(2) この結果，炉心熱伝達率は低くなり，発熱体被覆管の温度測定点におけるターンアラウンド時間，クエンチ時間は共に，基準試験より長くなった。

(3) 炉心における最高温度は1088Kであり，これは基準試験結果より50K高い。

本報告書は，電源開発促進対策特別会計法に基づき，科学技術庁からの受託によって行なった研究の成果である。

＊　原子力データセンタ

CONTENTS

目　　次

Table and Figure List

1. Introduction

The Cylindrical Core Test Facility (CCTF)[1] is an experimental facility designed to study the integral system behavior of a Pressurized Water Reactor (PWR) during the refill and the reflood phases of a postulated Loss-of-Coolant Accident (LOCA).

The objectives of the CCTF program are:

(1) Demonstration of effectiveness of Emergency Core Cooling (ECC) system in a PWR during the refill and the reflood phases,

(2) Provision of information for developing analytical methods of thermo-hydraulic behaviors in the system, and

(3) Verification of reflood analysis codes, REFLA which is one-dimensional code developed at JAERI, and TRAC which is three-dimensional code developed in the USA.

Test series Core-I was conducted with changing various parameters in order to investigate their effects on the integral system behavior.

The purpose of this work is to examine the effects of the loop flow resistance on the thermo-hydraulic behavior in the system during the reflood phase.

The increased loop flow resistance test was also performed in FLECHT-SET[2] and PKL[3]. The result of the FLECHT-SET test showed that the 35% increase of the loop flow resistance caused the about 15% decrease in the loop flow and the flooding rates, the longer turnaround and quench times. The percentage change of these was smaller than the percentage increase of the loop flow resistance. The temperature rise was only 12 K or 5% higher and the quench time extended by only 25 seconds or 8%.

In the PKL test, the loop flow resistance was increased remarkably.

The increasing rate was twice in the broken loop and more than three times in the intact loops. The temperature rise was 69 K or about 65% higher and the quench time at the midplane was 55 seconds or 83% longer. The remarkable increase of the loop flow resistances caused the significant effects on the core behavior.

For the purpose, the results of the increased flow resistance test (High K) are compared to those of the reference test (Base-case). The loop flow resistance for Base-case, C1-5, was referred from the FLECHT-SET facility design[2]. That for High K, C1-1, was about 40% higher than for the Base-case test.

2. Experimental Conditions

2.1 Facility design

The primary system of CCTF consists of a pressure vessel and four primary loops, as shown in Fig.2.1.

To simulate the system effect during refill and reflood phases of a postulated PWR LOCA, the following items were considered as the design criteria:

(1) The elevations of the components are kept as close to those of a PWR as possible,

(2) The length of each component flow path is also preserved,

(3) The flow areas of the components are scaled down in proportion to the scaling factor of core flow area, and

(4) The facility has three intact loops and one broken loop which simulates double-ended cold leg break.

The reference reactor is the Trojan reactor in the USA, and the Ohi reactor in Japan is partly referred.

The pressure vessel contains a core, upper and lower plena, and a downcomer. The core has thirty-two 8×8 bundles which simulate 15×15 type fuel assemblies including unheated rods. The core configration is shown in Fig.2.2.

The core has 1824 full-height electrically heated rods, as shown in Fig.2.3. An axial power distribution is chopped cosine. Each bundle has high, medium and low power heated rods.

The annular downcomer is shown in Fig.2.2. The core baffle region area in a PWR is scaled and included in the simulated downcomer flow area to reduce a small gap effect in a downcomer. The resulted gap size of the annulus is 61.5 mm.

The internals in the upper plenum consist of control rod guide tubes, support columns, short stubs, orifice plates and open holes, as shown in Fig.2.4 and Fig.2.5. These internals simulate those of a 17 × 17 type PWR. The radial dimensions of them are scaled down in proportion to the bundle array size.

The primary loop arrangement is shown in Fig.2.1. The loop consists of hot leg and cold leg pipings, an active steam generator, and a pump simulator, as shown in Fig.2.6. U-tubes in the steam generator are about 5 m shorter than actuals and those of two loops are housed in a single shell.

The flow resistance in the loop can be adjusted by the orifice plates in the pump simulator, as shown in Fig.2.7.

2.2 Test procedure and conditions

The test procedures were as follows: After establishing the initial conditions of the test, the electric power for the preheating was turned off and the lower plenum was filled with saturated water to a specified level. When the water level in the lower plenum reached 0.90 m and other initial conditions of the test stabilized, the electric power was applied to the heated rods in the core and the data recording was started. When a specified initial temperature was reached, direct injection of the accumulator water into the lower plenum was initiated. Decay of the power input to the rods was scheduled to begin when the water reached the bottom of the heated length of the rods. The specified initial clad temperature of the heated rods for the initiation of the coolant injection was predetermined by interpolation between the initial clad temperature and the clad temperature assumed for the

time of the core reflood initiation. The specified power decay is based on the decay curve of the ANS standard × 1.2 + ^{238}U capture decay at 30 seconds after shutdown.

When the assumed water level reached the specified height from the bottom of heated length, the injection port was changed from the lower plenum to the three intact cold leg ECC ports. At about 17 seconds after the initiation of the accumulator injection, the valves in the accumulator line and LPCI circulation line were closed and the valve in LPCI injection line was opened. These actions transferred the ECC injection from the accumualtor injection mode to LPCI mode.

The generated steam and the entrained water flowed via broken and intact loops to the containment tanks. The steam was then vented to the atmosphere to maintain the pressure in the containment tanks constant.

When all thermocouples on the surface of heated rods indicated temperature close to the saturated temperature, the power supply to the heated rods and the ECC injection were turned off, thus terminating the test.

The conditions of the High K and the Base-case tests are listed in Table 2.1 and Table 2.2, respectively. The test conditions of Base-case were based on results of typical safety analyses[1]. The major conditions of two tests were similar except the loop flow resistance.

The orifice diameter in the pump simulator was 95 mm$^{\phi}$ for Base-case and 85 mm$^{\phi}$ for High K. The pump flow resistance was about 1.7 times of that of Base-case, and the loop total flow resistance increased by about 40%. The K-factor listed in the table was difined as:

$$K = \frac{\Delta P_{pump}}{\frac{G^2}{2\rho}}$$

where ΔP : differential pressure through pump

G : mass velocity in loop piping

ρ : steam density at pump

Table 2.1 Test condition for C1-1

1. TEST TYPE : TEST C1-1 (CCTF MAIN TEST NO.1)
2. TEST NUMBER : RUN 01G 3. DATE : JUNE 21, 1979
4. POWER : A: TOTAL: 9.35 MW; B:LINEAR: 1.4 KW/M
5. RELATIVE RADIAL POWER SHAPE :

   A: ZONE: A B C

   B: RATIO: 1.08 1.0 0.82
6. AXIAL POWER SHAPE : CHOPPED COSINE
7. PRESSURE (KG/CM^2A) :

   A: SYSTEM: 2.07, B: CONTAINMENT 2.07,

   C: STEAM GENERATOR SECONDARY: 50
8. TEMPERATURE (DEG.C) :

   A: DOWNCOMER WALLS 188, B: VESSEL INTERNALS 117

   C: PRIMARY PIPING WALLS 122, D: LOWER PLENUM LIQUID 116

   E: ECC LIQUID 35,F: STEAM GENERATOR SECONDARY 263

   G: CORE TEMPERATURE AT ECC INITIATION 506
9. ECC INJECTION TYPE: C

   A: COLD LEG, B: LOWER PLENUM, C: LOWER PLENUM + COLD LEG
10. PUMP K-FACTOR : ~25 (UNCERTAIN)
11. ECC FLOW RATES AND DURATION :

    A: ACCUMULATOR 264 M^3/HR FROM 0 TO 21 SECONDS

    B: LPCI 30.6 M^3/HR FROM 21 TO 705.5 SECONDS

    C: ECC INJECTION TO LOWER PLENUM : FROM 0 TO 15.5 SECONDS

    (VALVE OPENING AND CLOSING TIMES ARE INCLUDED IN THE INJECTION DURATION)
12. INITIAL WATER LEVEL IN LOWER PLENUM : 0.87 M.
13. POWER CONTROL : ANS x 1.2 + ACTINIDE (30 SEC AFTER SCRAM)
14. EXPECTED BOCREC TIME FROM ECC INITIATION 12 SEC
15. EXPECTED PEAK TEMPERATURE AT BOCREC 600 C

Table 2.2 Test condition for C1-5

1. TEST TYPE : TEST C1-5 (CCTF MAIN TEST NO.5)
2. TEST NUMBER : RUN 014 3. DATE : Oct.19, 1979
4. POWER : A: TOTAL: 9.36 MW; B:LINEAR: 1.40 KW/M
5. RELATIVE RADIAL POWER SHAPE :

   A: ZONE: A B C

   B: RATIO: 1.07 : 1.0 : 0.82
6. AXIAL POWER SHAPE : CHOPPED COSINE
7. PRESSURE (KG/CM^2A) :

   A: SYSTEM: 2.02, B: CONTAINMENT 1.99,

   C: STEAM GENERATOR SECONDARY: 50
8. TEMPERATURE (DEG.C) :

   A: DOWNCOMER WALL 182, B: VESSEL INTERNALS 115,

   C: PRIMARY PIPING WALL 120, D: LOWER PELNUM·LIQUID 114,

   E: ECC LIQUID 39, F: STEAM GENERATOR SECONDARY 262,

   G: CORE TEMPERATURE AT ECC INITIATION 502
9. ECC INJECTION TYPE: C

   A: COLD LEG, B: LOWER PLENUM, C: LOWER PLENUM + COLD LEG
10. PUMP K-FACTOR : ~ 15
11. ECC FLOW RATES AND DURATION :

    A: ACCUMULATOR 278 M^3/HR FROM 0 TO 23.5 SECONDS

    B: LPCI 30.2 M^3/HR FROM 23.5 TO 685.5 SECONDS

    C: ECC INJECTION TO LOWER PLENUM : FROM 0 TO 14.5 SECONDS

    (VALVE OPENING AND CLOSING TIMES ARE INCLUDED IN THE INJECTION DURATION)
12. INITIAL WATER LEVEL IN LOWER PLENUM : 0.87 M.
13. POWER CONTROL : ANS x 1.2 + ACTINIDE (30 SEC AFTER SCRAM)
14. EXPECTED BOCREC TIME FROM ECC INITIATION 12 SEC
15. EXPECTED PEAK TEMPERATURE AT BOCREC 600 C

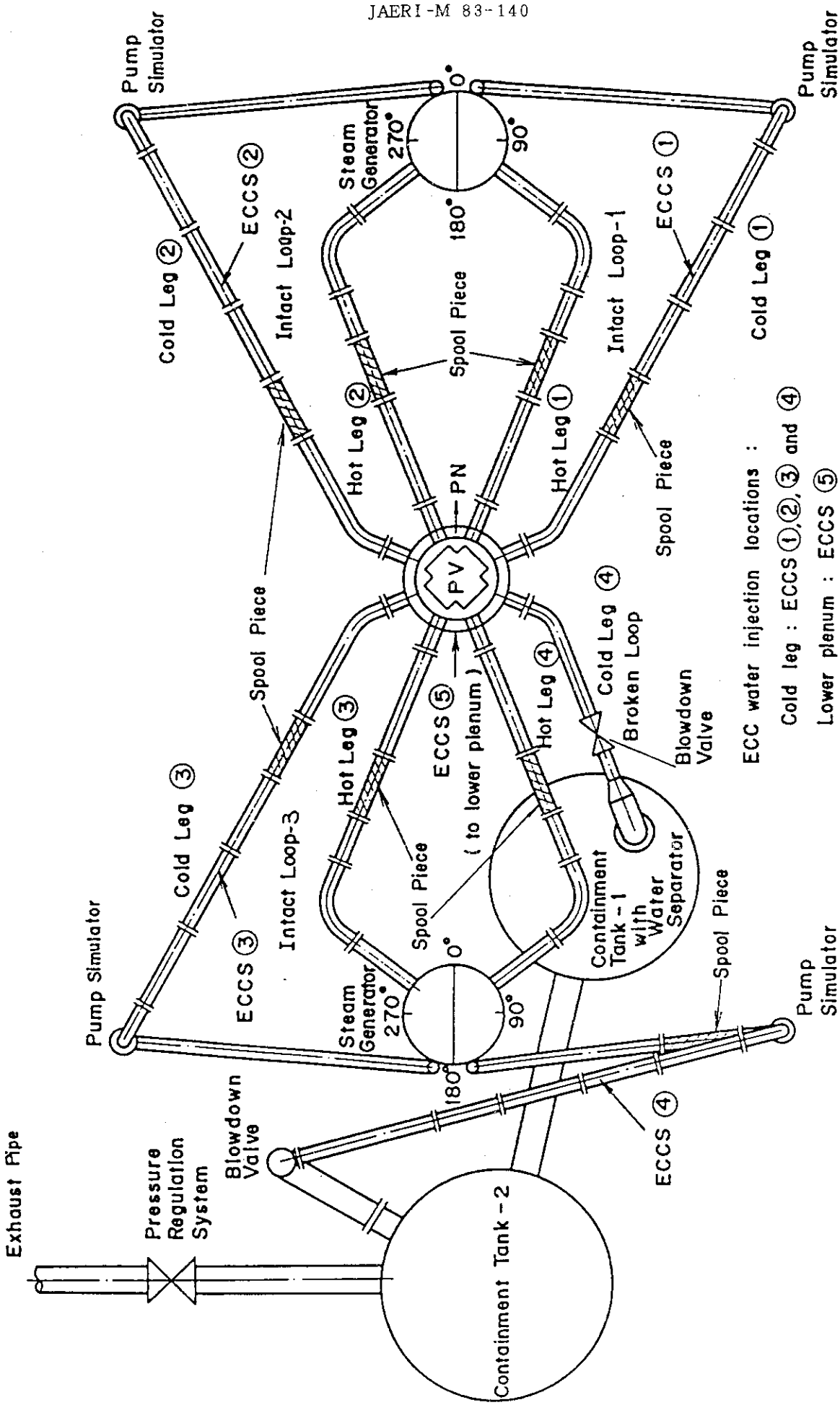

Fig.2.1 Primary loop piping

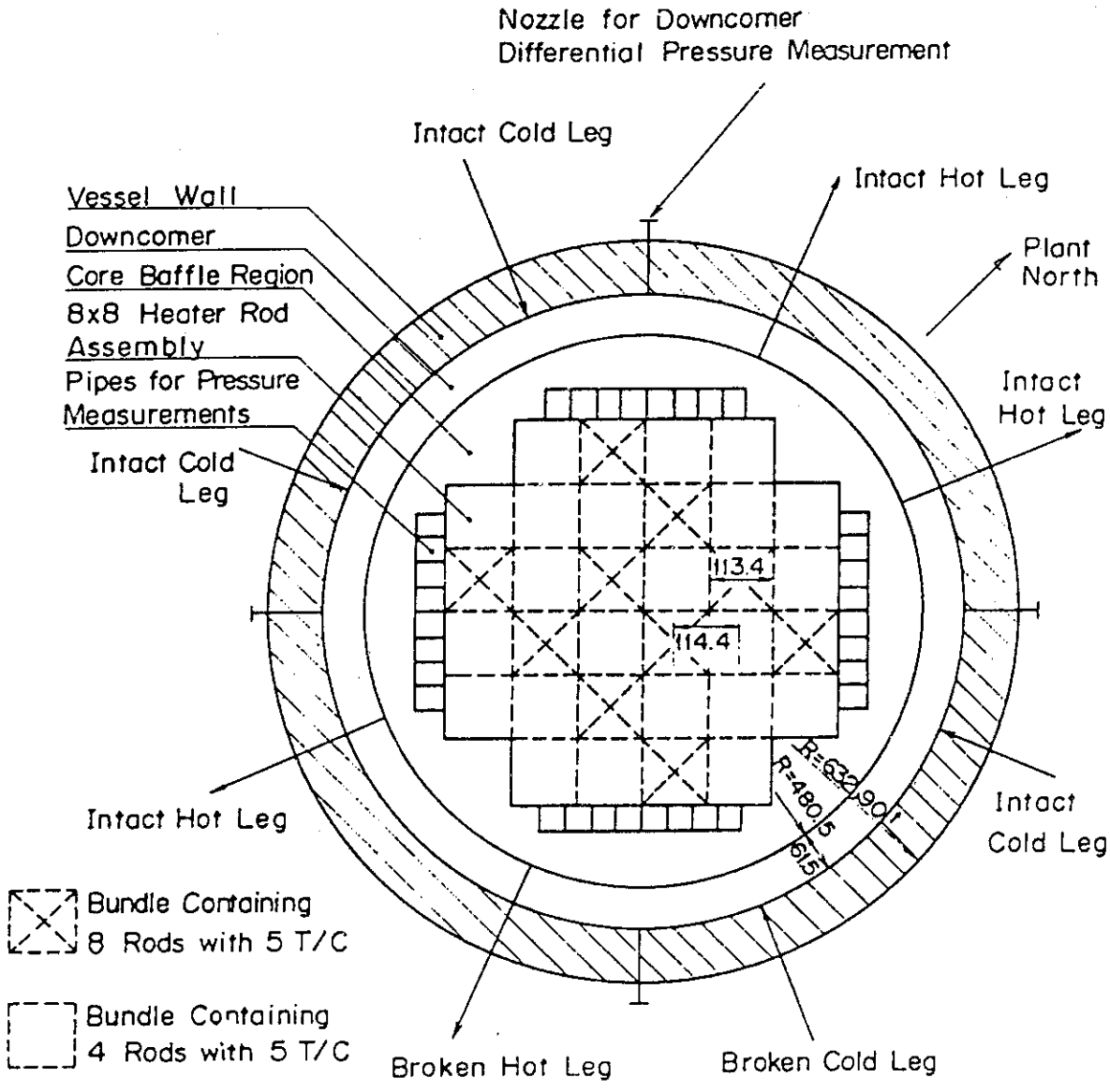

Fig.2.2 Cross section of pressure vessel

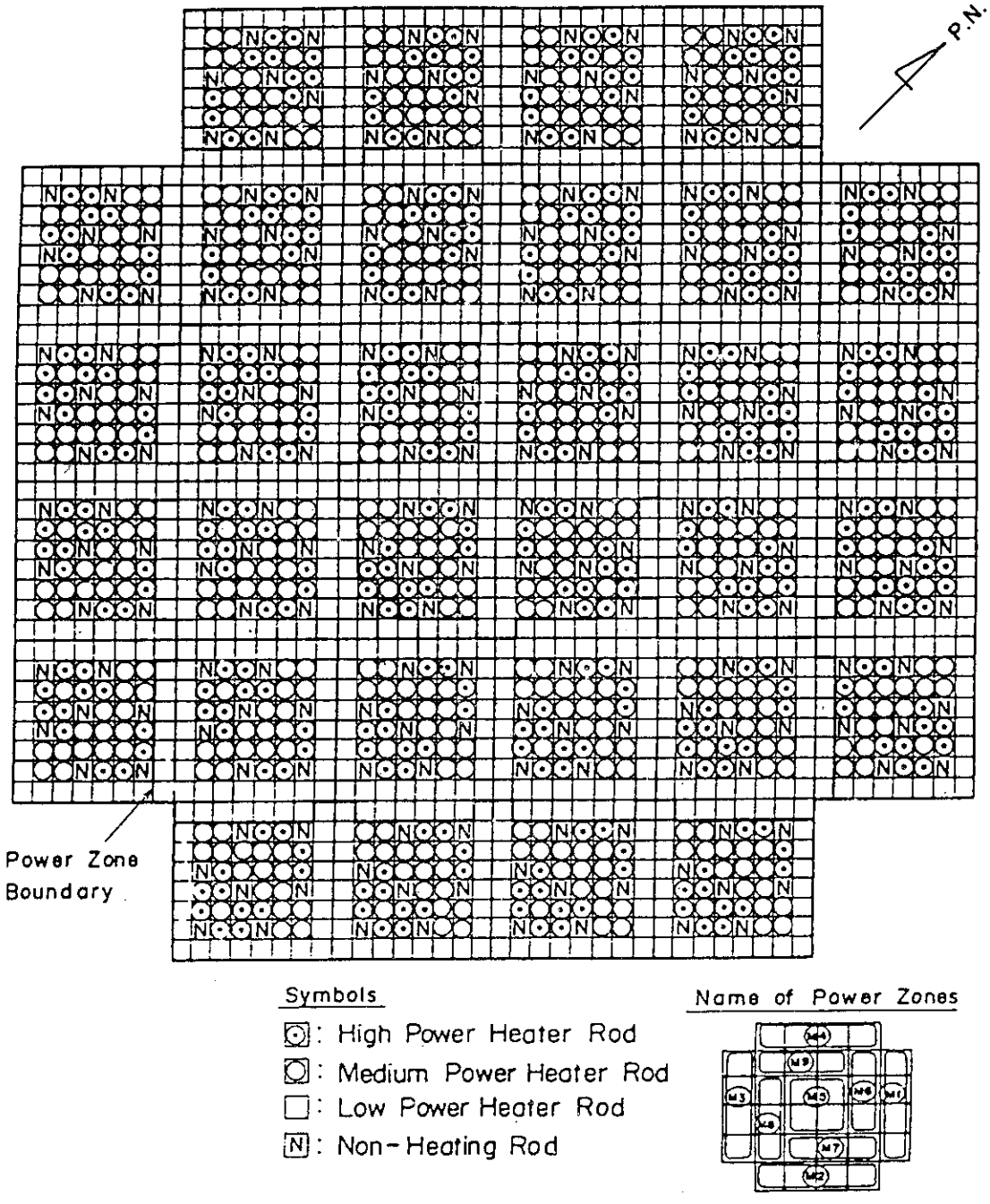

Fig.2.3 Heater rod

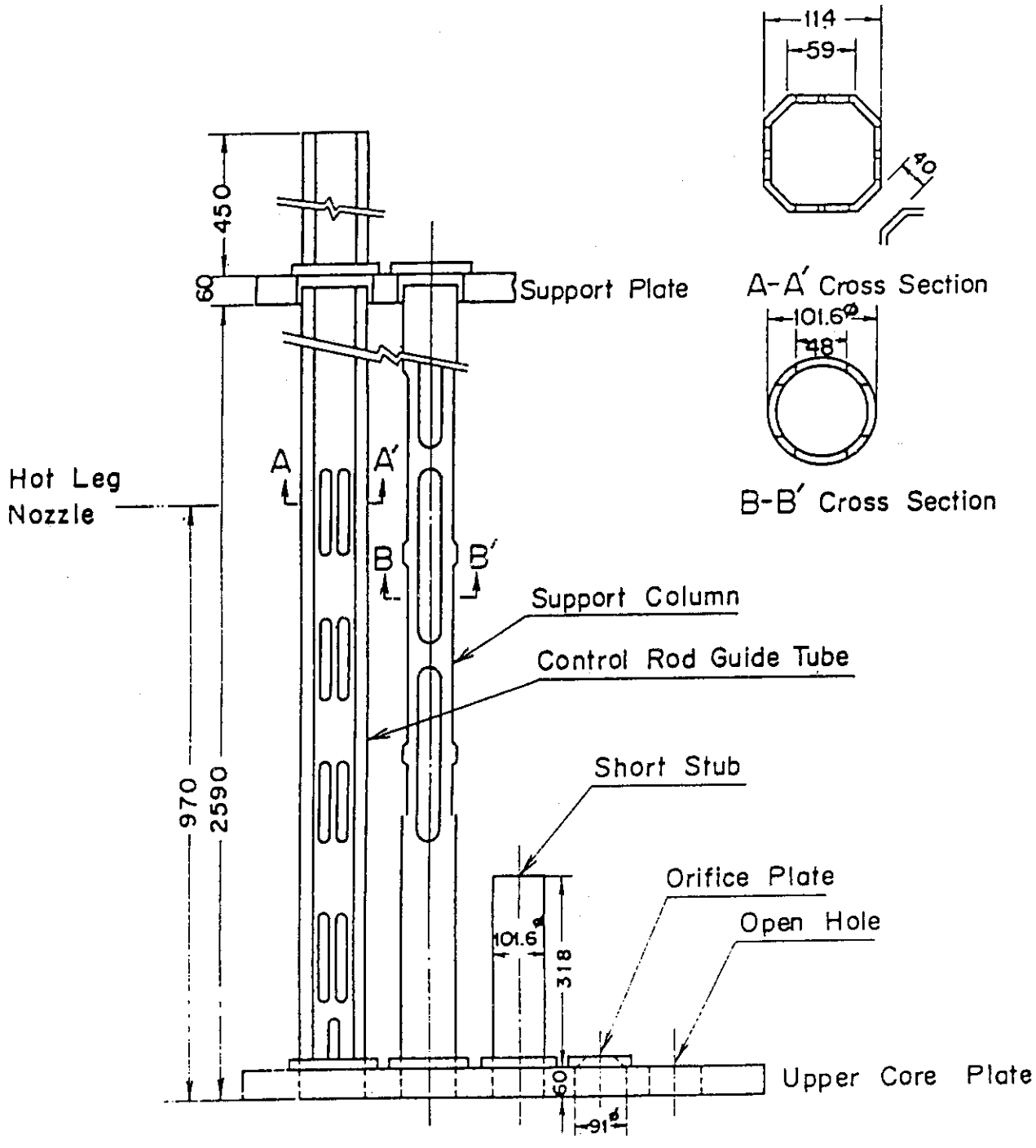

Fig.2.4 Conception of internals

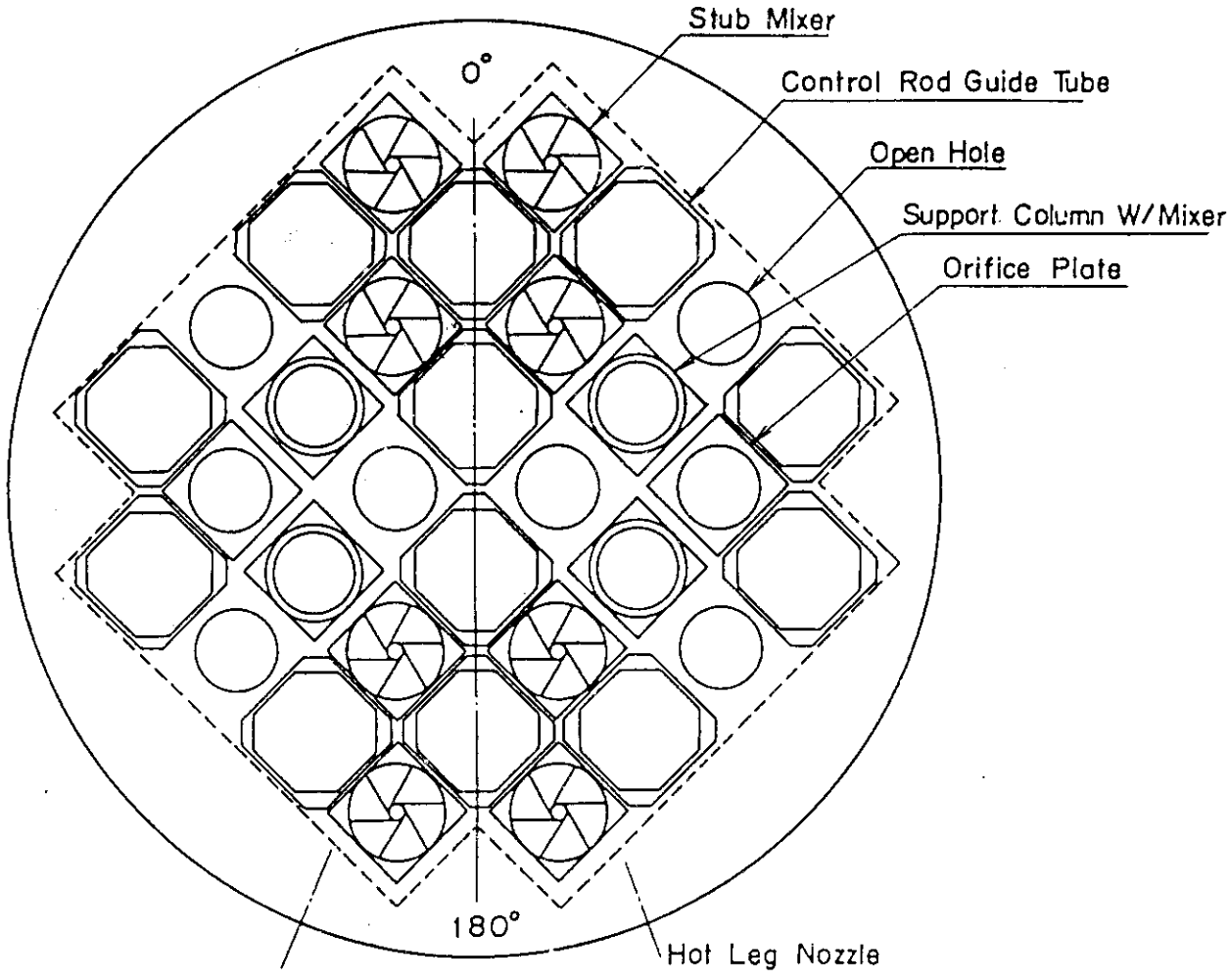

Fig.2.5 Arrangement of internals

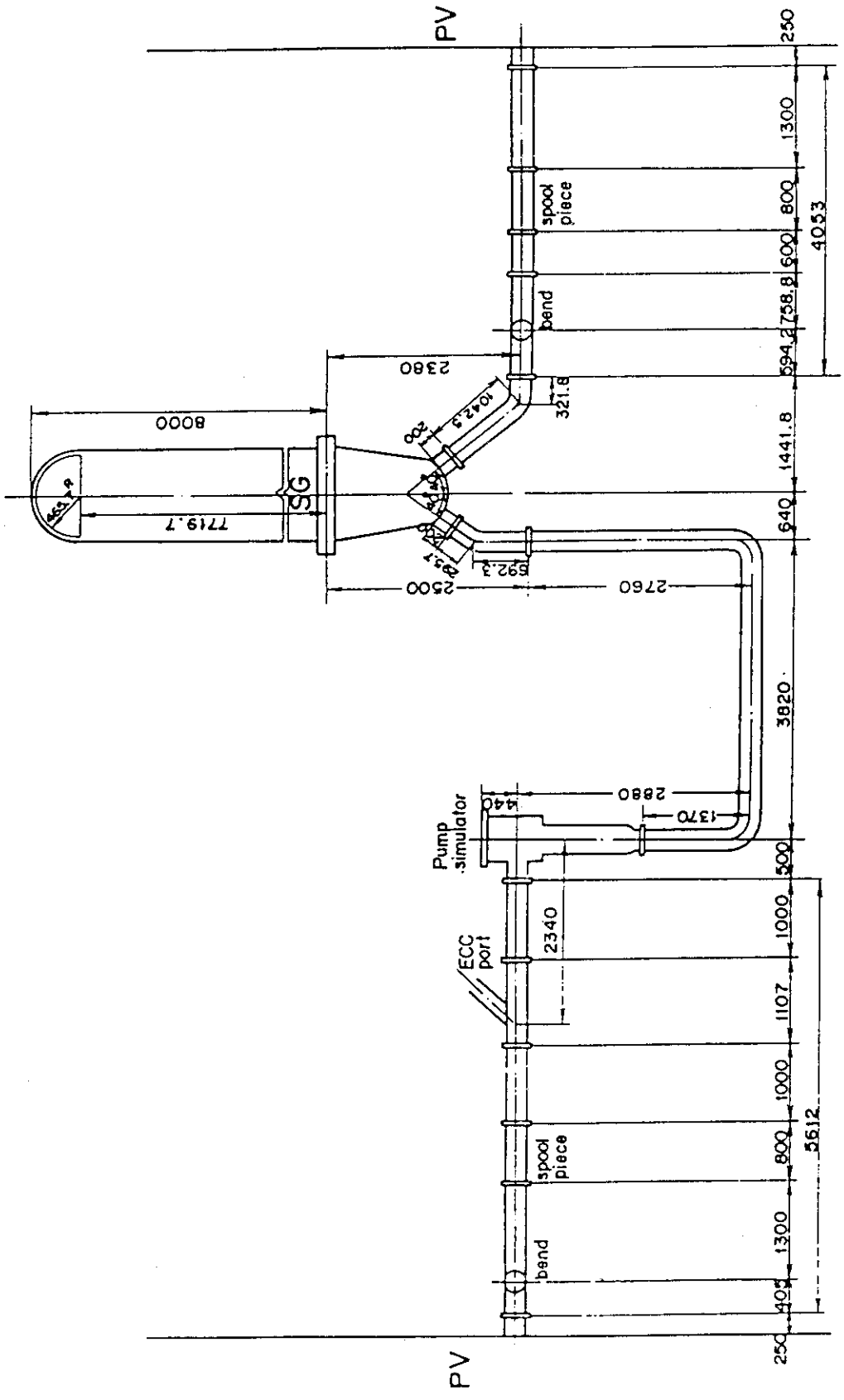

Fig.2.6 Primary loop

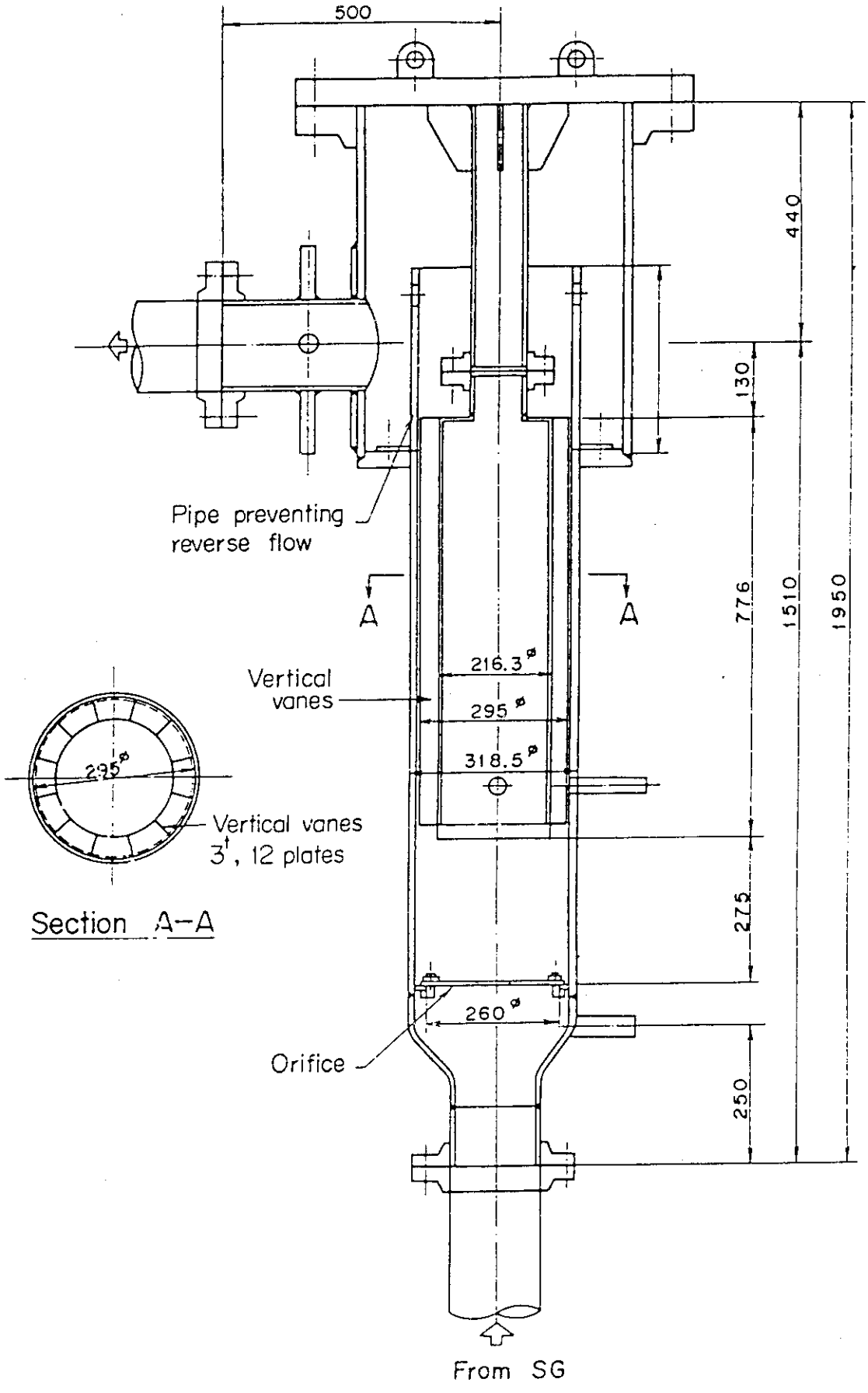

Fig.2.7 Pump simulator

3. Results and Discussion

3.1 System behavior

○ Vessel differential pressure

The core and the downcomer differential pressures are compared between High K and Base-case in Fig.3.1. Since the frictional and the acceralational pressure drops are negligible in the vessel[1], the differential pressure is equivallent to the static water head of the accumulated water. During the accumulator injection period, the injected water accumulated in the core and the downcomer, so that the differential pressures in the downcomer and the core are nearly identical. After reduction of the ECC injection rate, the downcomer differential pressure increases gradually during first 100 seconds, and stays at nearly constant value after that. This value is very close to the downcomer overflow level. The tendencies of the differential pressure responses of the downcomer and the core in the present test are similar to those of Base-case, though the value of the core differential pressure is slightly lower for High K than for Base-case.

○ Flow behavior in loops

The loop differential pressures are compared between two tests in Fig.3.2. The differential pressures of the intact loops in each test are almost identical, so that one of those is presented in the figure. The differential pressure of the intact loop is slightly higher for High K than for Base-case. This tendency is not observed in the comparison of the broken loop differential pressures. It will be discussed later.

The calculated mass flow rates through the loops are shown in Fig.3.3. The mass flow rates through the intact and broken loops are

about 20% lower for High K than for Base-case. In a system effect test, the driving force for the loop mass flow is the difference between the differential pressures of the downcomer and the core with ignoring the accumulated water head in the upper plenum. As shown in the previous figure, the value of each differential pressure for High K is roughly similar to that for Base-case. The higher loop flow resistance under the similar driving force caused the lower loop mass flow rate for High K. Then, the steam generation in the core was suppressed and resulted in the slightly lower core differential pressure for High K. And the intact loop differential pressure balanced with the core and the downcomer differential pressures at the slightly higher value for High K than for Base-case.

o Pressure drop at the broken cold leg nozzle

Figure 3.4 presents the differential pressure in the broken cold leg nozzle. The generated steam in the core flowed through the intact loops and the broken loop. The steam flowed through the intact loops was vented to containment tank-1 through the broken cold leg nozzle. The lower mass flow rates through the intact loops in High K caused the lower differential pressure in the broken cold leg nozzle in an early transient. The differential pressure for High K increases steeper after 85 seconds. At that time, the water level in the downcomer carry-over tank (containment tank-1) indicates the initiation of the water accumulation, as shown in Fig.3.5, and the downcomer differential pressure was close to the maximum value. According to the flow observation at the broken cold leg nozzle with video cameras, the carryover from the downcomer was observed even in an early transient, however, water

fraction appeared to significantly increase after about 80 seconds. These facts support that the downcomer overflow was initiated at 80 seconds, and the mixture of water and steam increased the pressure drop at the broken cold leg nozzle. For Base-case, the earlier initiation of the carryover from the downcomer is observed in Fig.3.5. The flow observation at the broken cold leg in Base-case also revealed that the significant carryover initiated at about 15 seconds. It is thought that the higher mass flow rate in the intact loops in Base-case caused the earlier carryover initiation and resulted in the higher pressure drop across the broken cold leg.

In a system effect test, this pressure drop directly affects the pressure in the vessel. The broken loop differential pressure, which is the difference between the upper plenum and containment tank-2 pressures, is also affected by the pressure drop across the broken cold leg nozzle. This is the reason why the tendency of the broken loop differential pressure was not similar to that of the intact loop one.

3.2 Core behavior

The comparison of the differential pressure in the upper plenum is shown in Fig.3.6. These differential pressures represent the accumulated water head in the upper plenum. The water accumulation for High K is about a half of that for Base-case. It is considered that the less mass flow rates through the loops for High K reduced the carryover water mass from the core and resulted in less water de-entrainment in the upper plenum.

The flooding rates of High K and Base-case are compared in Fig.3.7. The flooding rate for High K is about 20% lower than that for Base-case.

According to the mass balance calculation of the core, the flooding rate is the sum of the mass accumulation rates in the core and upper plenum, and the mass flow rates in the four loops, however, the mass accumulation rates in the core and the upper plenum were negligible as comparing with the loop flow rates except for an early reflood transient. Therefore, the about 20% lower mass flow rates in the loops for High K resulted in the about 20% lower flooding rate.

Figure 3.8 shows the comparison of the saturation temperature and the water temperature at the core inlet. The saturation temperature for High K is nearly the same as that for Base-case and the tendency and the value of the inlet water temperature for High K are very similar to those for Base-case. Those indicate that the boundary condition of the core was similar between two tests except for the flooding rate and the steam flow rates.

Figure 3.9 shows the comparison of the temperature responses of the maximum powered rod in the core. The temperature is higher in High K than in Base-case and the extended turnaround and quench times are observed in High K.

Figure 3.10 shows the turnaround times of the maximum powered rod. The significantly delayed turnaround is observed in High K at the elevations of 2.44 and 3.05 m. The turnaround times of the midplane (1.83 m elevation) are slightly longer than those of Base-case. The turnaround temperatures of the maximum powered rods are compared in Fig.3.11. Though the initial temperatures are almost identical, the turnaround temperature is about 50 K higher in High K than that of Base-case except the lower portion of the core. The maximum temperature rise at the midplane of High K is 210 K, which is 31% higher than that of Base-case.

The quench times of the maximum powered rods are shown in Fig.3.12. The effect of the loop flow resistance is weak at the elevations below the midplane. The quench times at the higher elevations are longer for High K than for Base-case. This trend is significant at the 3.05 m elevation. In Base-case, four of six quench times at the 3.05 m elevation are shorter than the quench times at the 2.44 m elevation where as only two are shorter in High K. The lower water accumulation in the upper plenum of High K may affect the quench front propagation from the top of the core. The maximum quench time at 2.44 m elevation for High K is 65 seconds or 13% longer than that for Base-case.

Figure 3.13 shows the comparison of the void fractions in the core. The quench times at the elevations of 1.015, 1.83 and 2.44 m in High K, as shown by arrows, are about 120 seconds, 330 seconds and 500 seconds, respectively. It is found that the void fraction above the quench front is higher in High K than that of Base-case.

Figure 3.14 shows the comparison of the heat transfer coefficients of the maximum powered rod at 1.83, 2.44 and 3.05 m elevations. The heat transfer coefficient at each elevation is significantly lower in High K than in Base-case. The comparison of the core pressure, as shown in Fig.3.15, indicates no significant difference, and the water temperature at the core inlet of High K was similar to that of Base-case, so that the contribution of them to the difference of the heat transfer coefficients can be ignored. It is considered that the lower flooding rate for High K caused the higher void fraction above the quench front and reduced the heat transfer coefficient. The lower heat transfer coefficient resulted in the higher turnaround temperature and the longer turnaround and quench times for High K.

The increasing rate of the loop resistance in CCTF was bigger than

that in FLECHT-SET and smaller than that in PKL, and the changing rates of the temperature rise and the quench time in CCTF are bigger than in FLECHT-SET and smaller than PKL. Since the run conditions are not the same between the three facility tests, the results cannot be compared directly. However, it is found that the effect of the flow resistance is rather significant on the temperature rise than on the quench time.

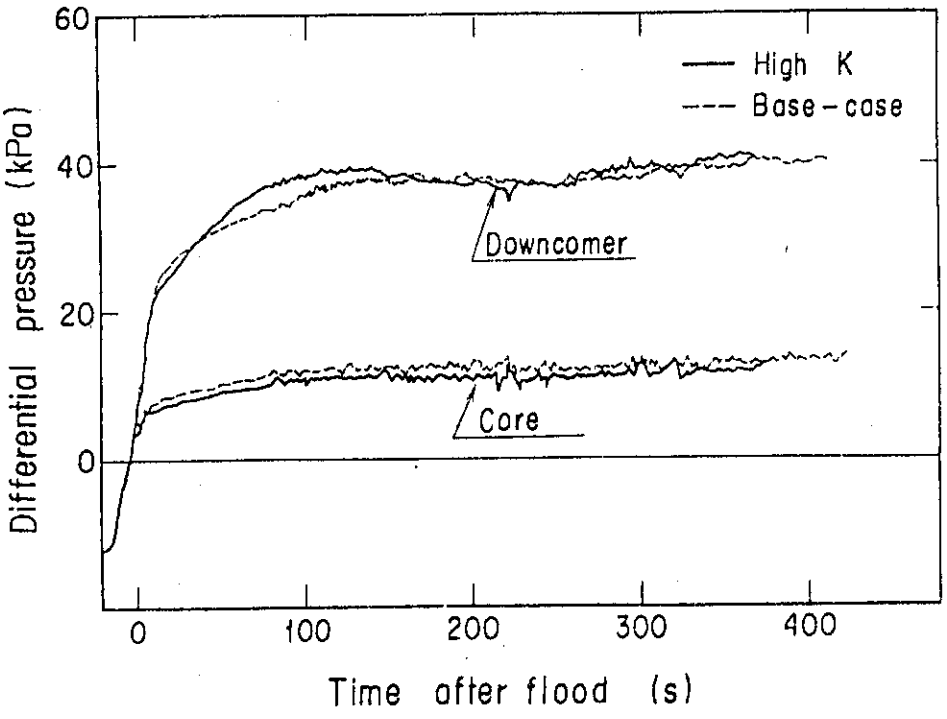

Fig.3.1 Differential pressure through downcomer and core

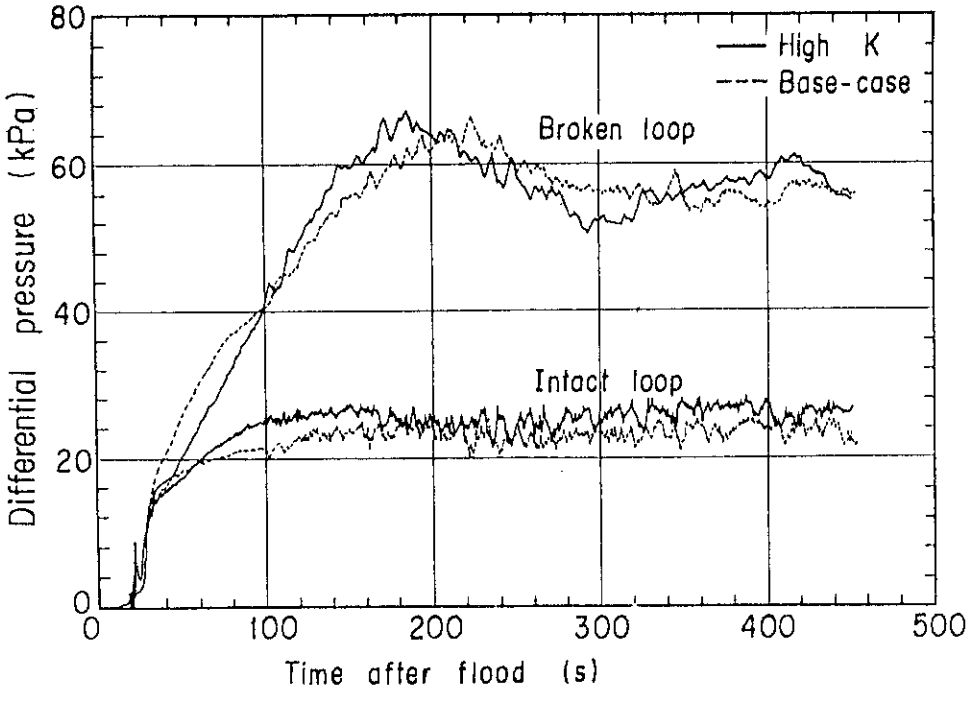

Fig.3.2 Differential pressures of intact and broken loops

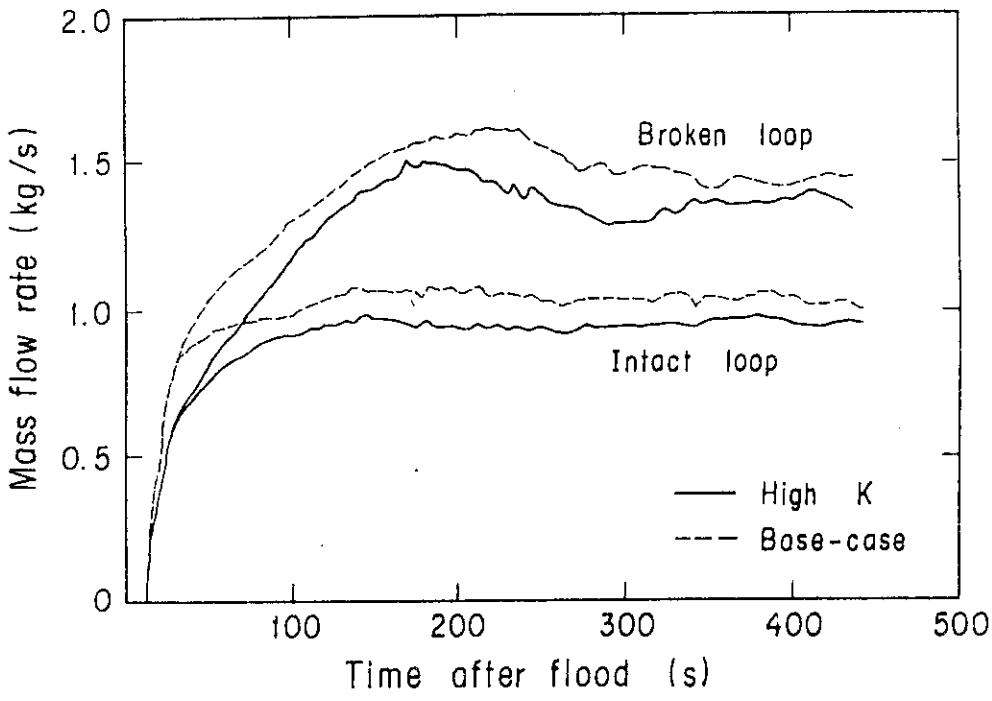

Fig.3.3 Mass flow rates in intact and broken loops

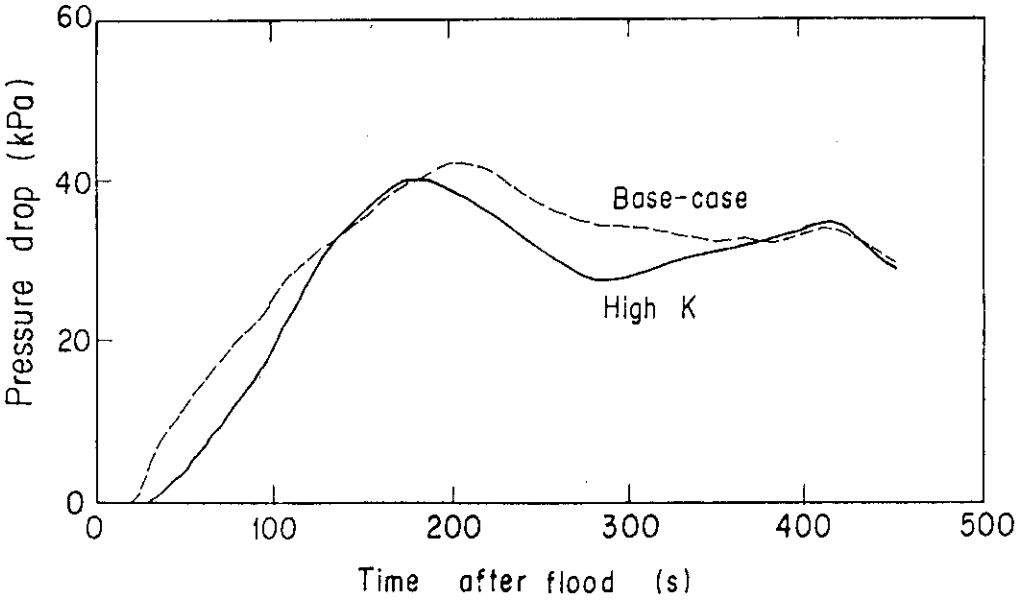

Fig.3.4 Differential pressure of broken cold leg

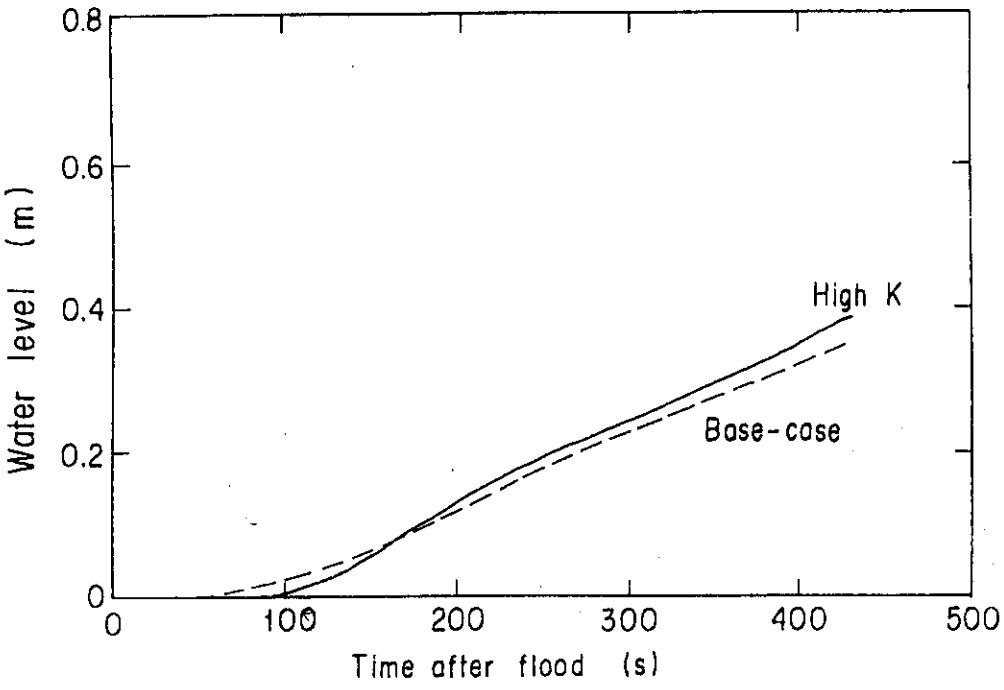

Fig.3.5 Water level in downcomer overflow tank

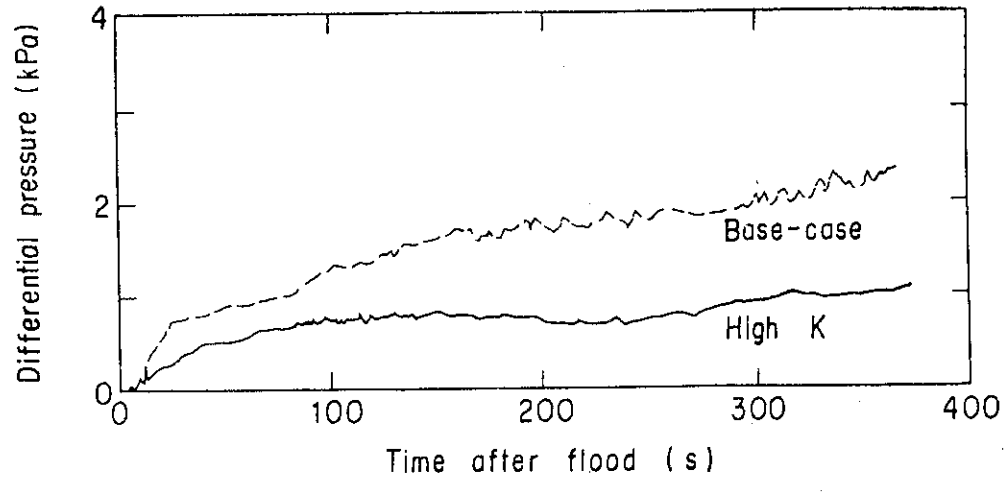

Fig.3.6 Comparison of water accumulation in upper plenum

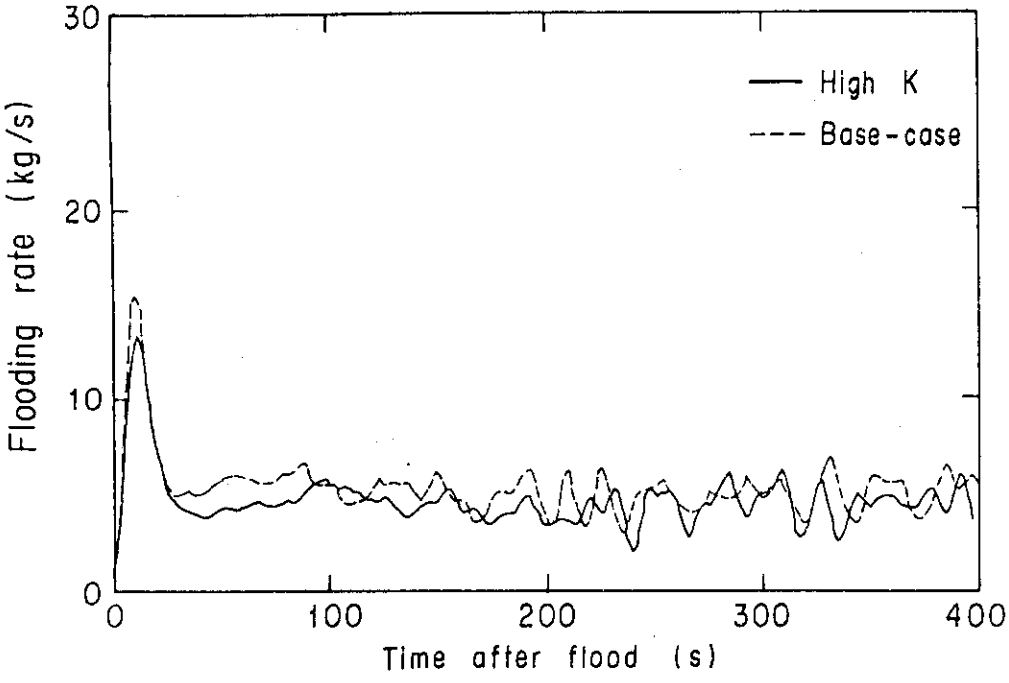

Fig.3.7 Comparison of flooding rate

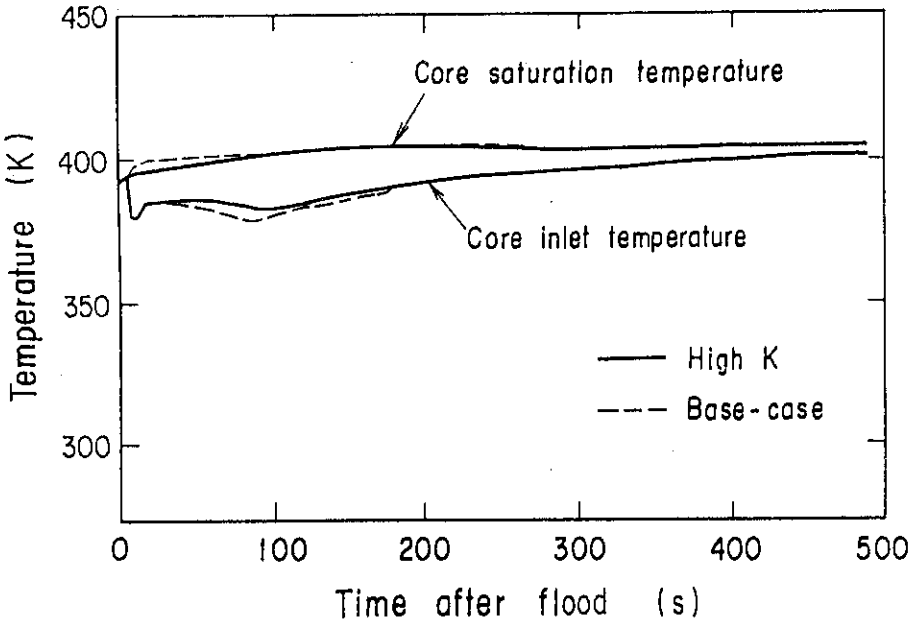

Fig.3.8 Core inlet temperature and core saturation temperature

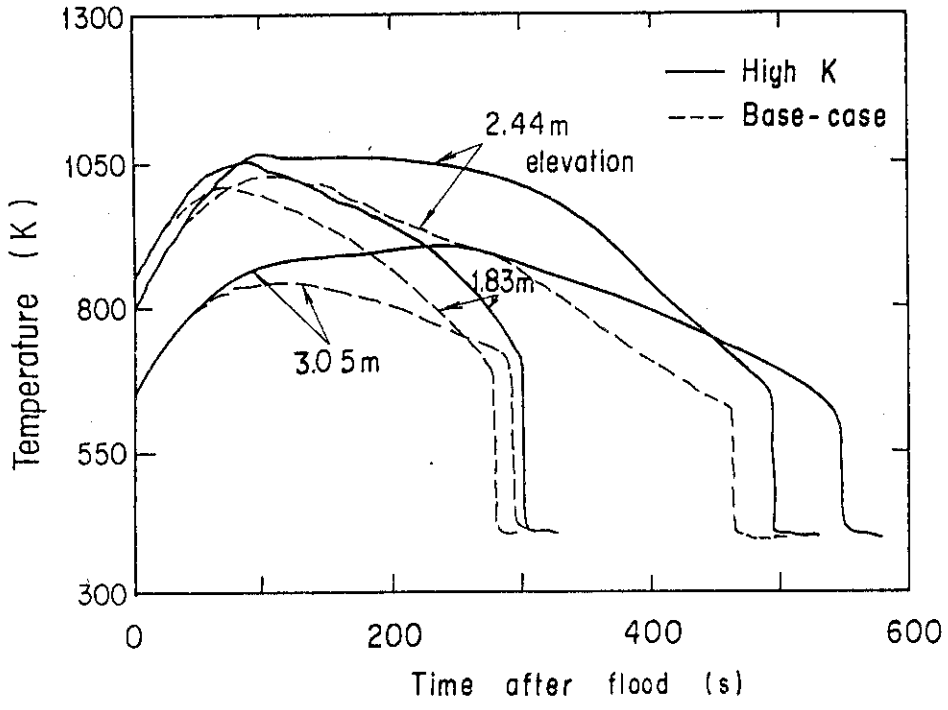

Fig.3.9 Temperature response of upper half of high powed rod in A region

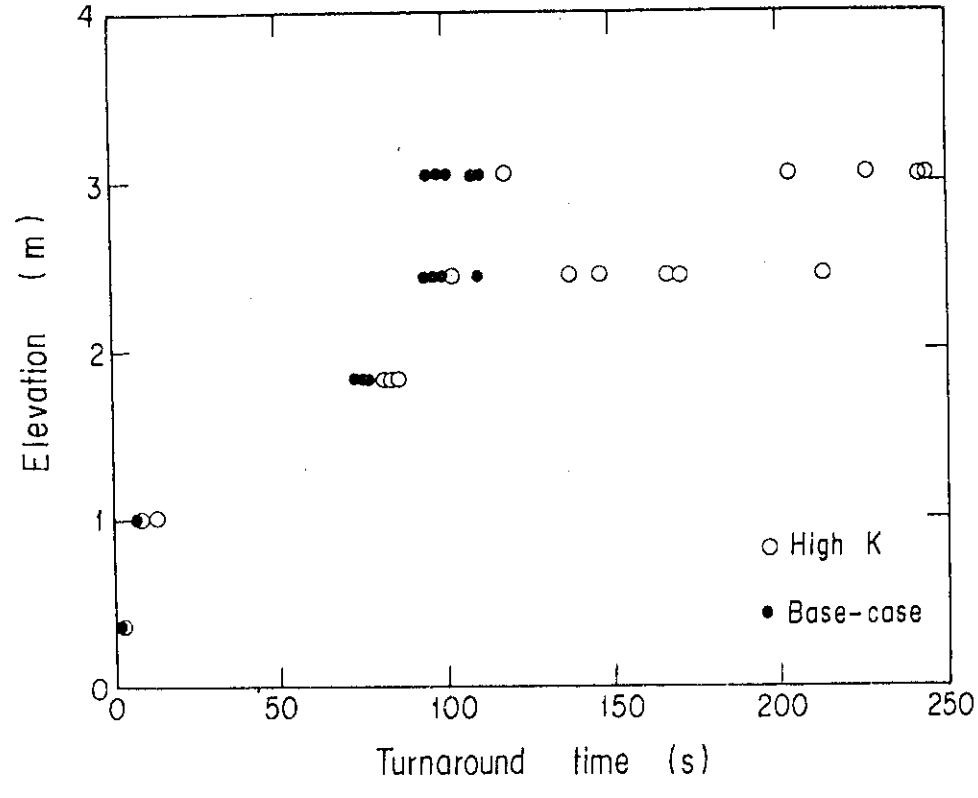

Fig.3.10 Comparison of turnaround times of maximum powered rod

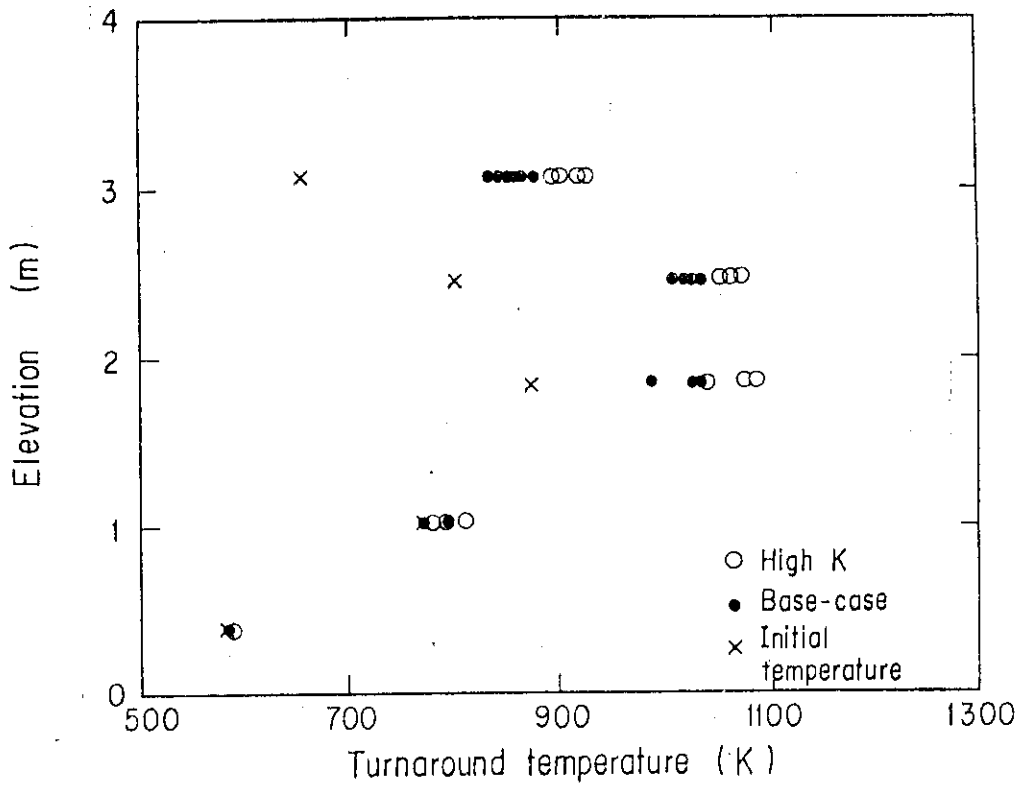

Fig.3.11 Comparison of turnaround temperatures of maximum powered rod

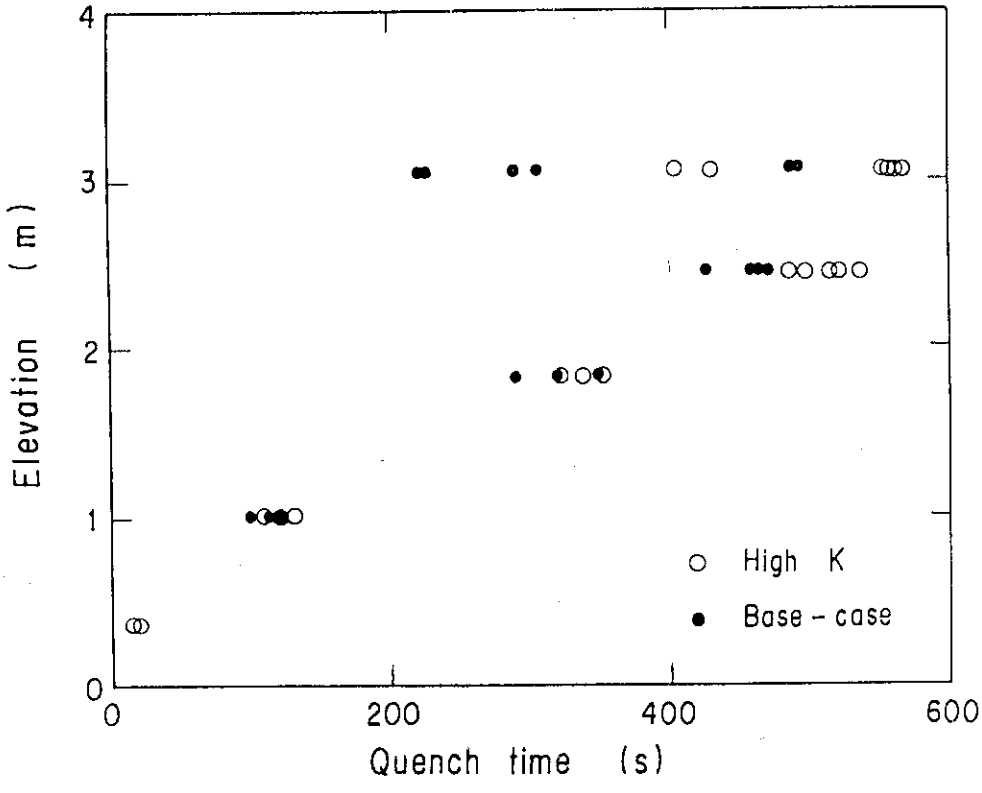

Fig.3.12 Comparison of quench times of maximum powered rod

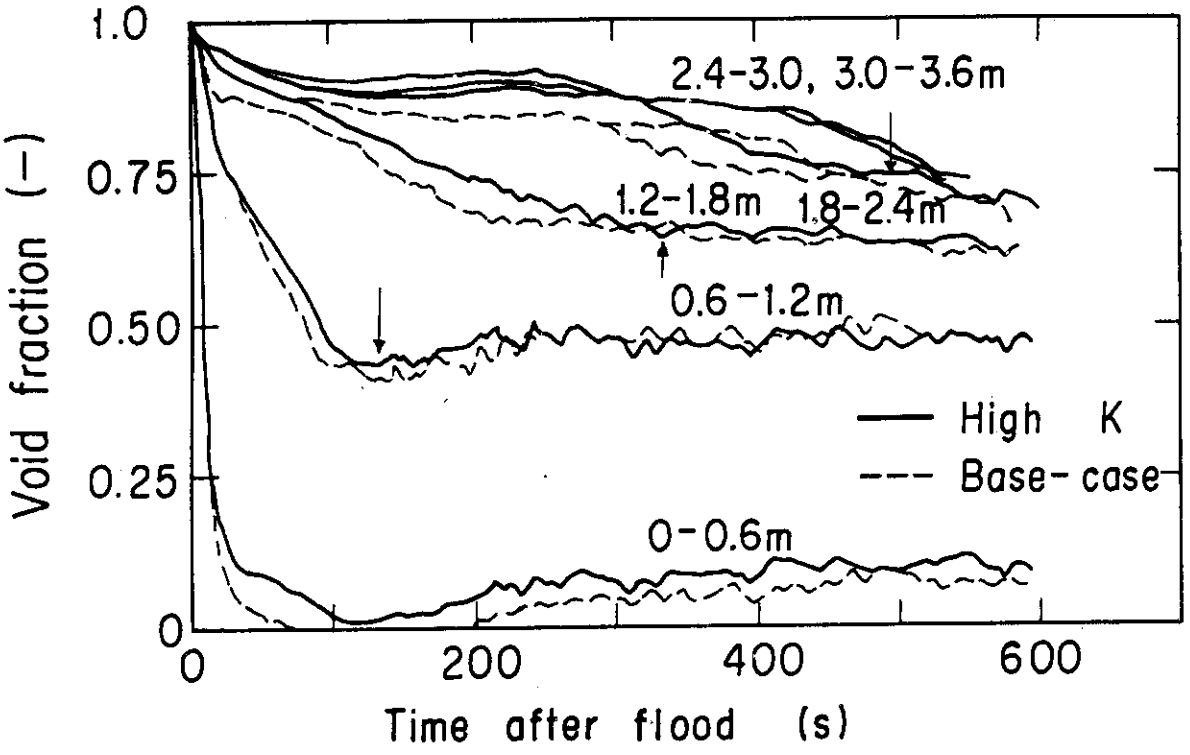

Fig.3.13 Void fraction in core

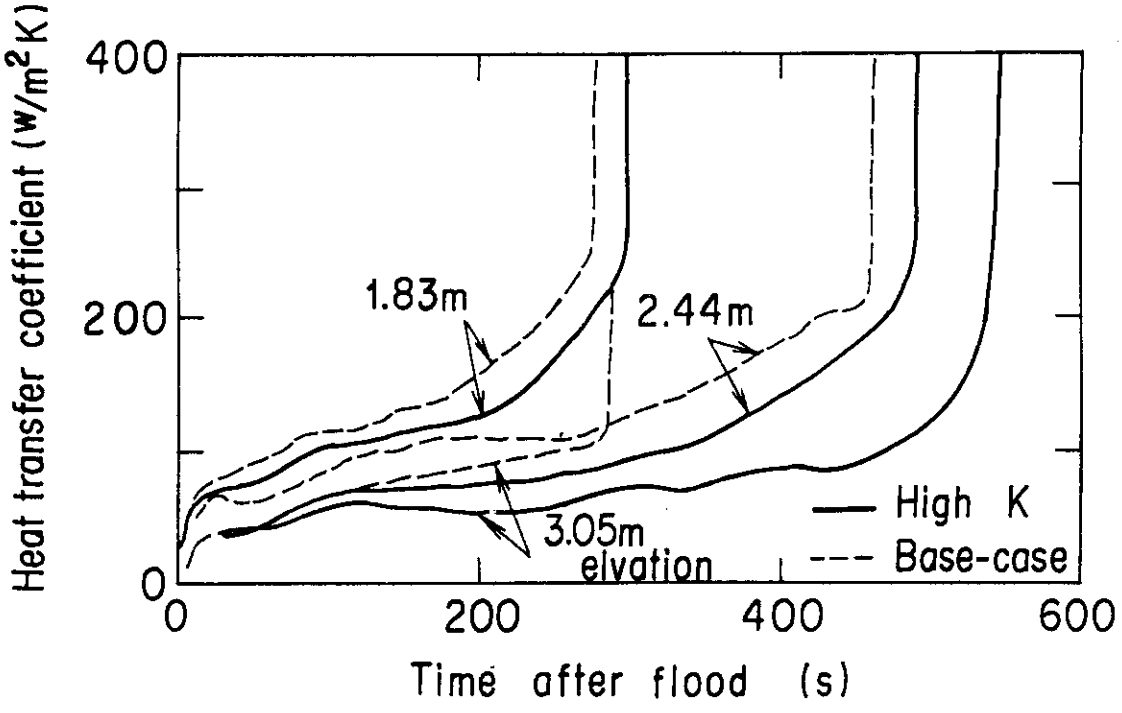

Fig.3.14 Comparison of heat transfer coefficient

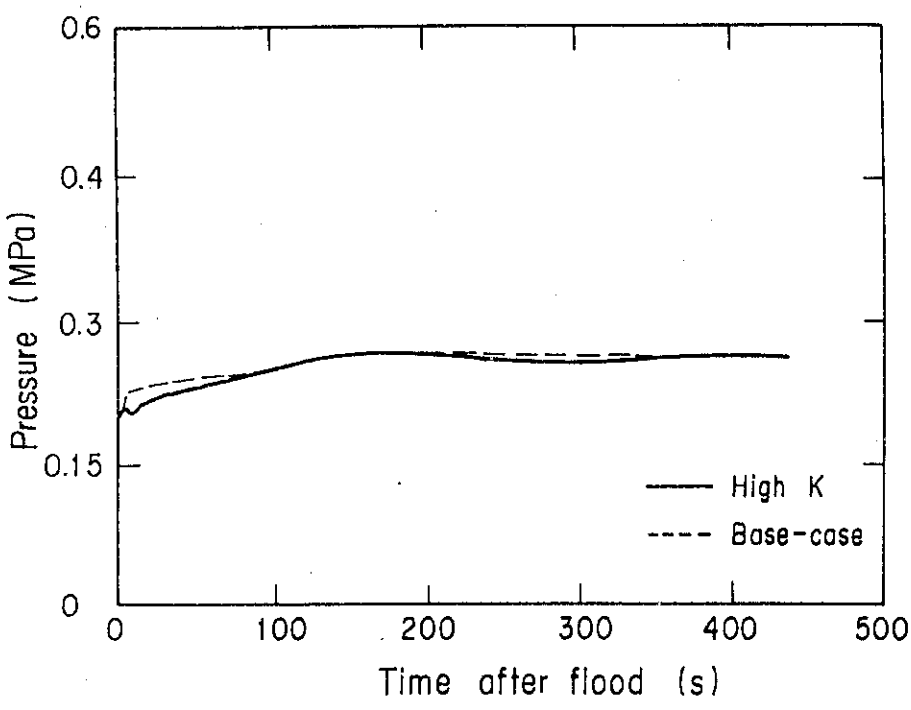

Fig.3.15 Comparison of core pressure

4. Conclusions

The effects of the loop flow resistance on the reflood phenomena in the CCTF test were investigated and the following conclusions were obtained.

(1) The effects on the differential pressures across the components in the system were weak, however, the 40% increased loop flow resistance reduced the steam flow rated through the loops by about 20 %, and caused about 20% lower core flooding rate.

(2) Induced lower heat transfer rate in the core caused the higher temperature rise and the longer quench time.

(3) Above result was consistent with the PKL and the FLECHT-SET results under considering the increasing rate of the loop flow resistance.

Acknowledgement

The authors are very grateful to Dr. M. Nozawa, Deputy Director General of Tokai Research Establishment, JAERI, Dr. S. Katsuragi, Director of Nuclear Safety Research Center, and Dr. K. Hirano, Deputy Director of Department of Nuclear Safety Research for their hearty suggestion and encouragement.

They are deeply indebted to Mr. T. Iguchi, Mr. J. Sugimoto, Dr. H. Akimoto, and Mr. T. Okubo for their analytical support. They would like to express their appreciation to Mr. H. Adachi, Dr. Y. Sudo, Mr. M. Sobajima, Mr. T. Iwamura, Mr. M. Osakabe, and Mr. A. Ohnuki for their useful discussions, Messrs. K. Sekiguchi, Y. Fukaya, N. Suzuki, T. Oyama, T. Wakabayashi, Y. Niitsuma, J. Matsumoto, T. Nishikizawa, and H. Sonobe for their contribution to the facility operation, to Messrs. R.K. Fujita and D.H. Miyasaki, resident engineers from USNRC, and to Dr. P.J. Schally, resident engineer from BMFT, for their devoted help.

References

1) Murao, Y., et al.: Evaluation report on CCTF Core-I reflood test C1-5 (Run 14), JAERI-M 83-027, (1983).

2) Waring, J.P. and Hochreiter, L.E.: PWR FLECHT-SET Phase B1 evaluation report, WCAP-8583, (1975).

3) Kirmse, R., et al.: Zusammenfassende Darstellung von Wichtigen Ergenbnissen der PKL Versuche der Testserien IA und IB (in German), CRS-A-360, (1979).

Appendix A

Definition of Tag. IDs in Appendix B

Figure list

1. Definition of Tag.ID for clad surface temperatures

Notation : TENNWAM

NN : Bundle number

WA : Power zone

WA = X1, X2 : High power (Local power factor 1.1)

WA = Y1, Y2 : Medium power (Local power factor 1.0)

WA = Z1, Z2 : Low power (Local power factor 0.95)

M : Elevation

	Elevation (m)	Axial power factor
1	0.38	0.568
2	1.015	1.176
3	1.83	1.492
4	2.44	1.312
5	3.05	0.815

2. Definition of power zone and bundle number

See Fig. A-1

3. Definition of Tag.ID for void fraction

See Fig. A-2

4. Definition of Tag.ID for average linear power of heater rod in each power unit zone

See Fig. A-3

5. Definition of carry-over rate fraction (C.R.F)

$$CRF = \frac{\dot{m}_{UP} + \dot{m}_{L}}{\dot{m}_{CR} + \dot{m}_{UP} + \dot{m}_{L}}$$

The calculated data within ±25 s are averaged:

$$(CRF)_i = \frac{1}{101} \sum_{k=i-50}^{i+50} (CRF)_k$$

where

ΔP_{UP} : Average of measured data at four orientations

ΔP_{CR} : Same as above

$$\dot{m}_{UP} = A_{up} \frac{d}{dt} (\Delta P_{UP})$$

$$\dot{m}_{CR} = A_{CR} \frac{d}{dt} (\Delta P_{CR})$$

$$\dot{m}_L = \sum_{k=1}^{4} \dot{m}_{pk}$$

$\dot{m}$: mass flow rate or mass accumulation rate

ΔP: differential pressure

suffix

UP: upper plenum

CR: core

L : loop

p : primary pump

6. Definition of Tag.ID for differential pressure through downcomer, upper plenum, core and lower plenum

See Fig. A-4

7. Definition of Tag.ID for differential pressure through intact and broken loop and broken cold leg nozzle

See Fig. A-5

8. Definition of Tag.ID for fluid temperature in inlet and outlet plenum and secondary of steam generator

See Fig. A-6

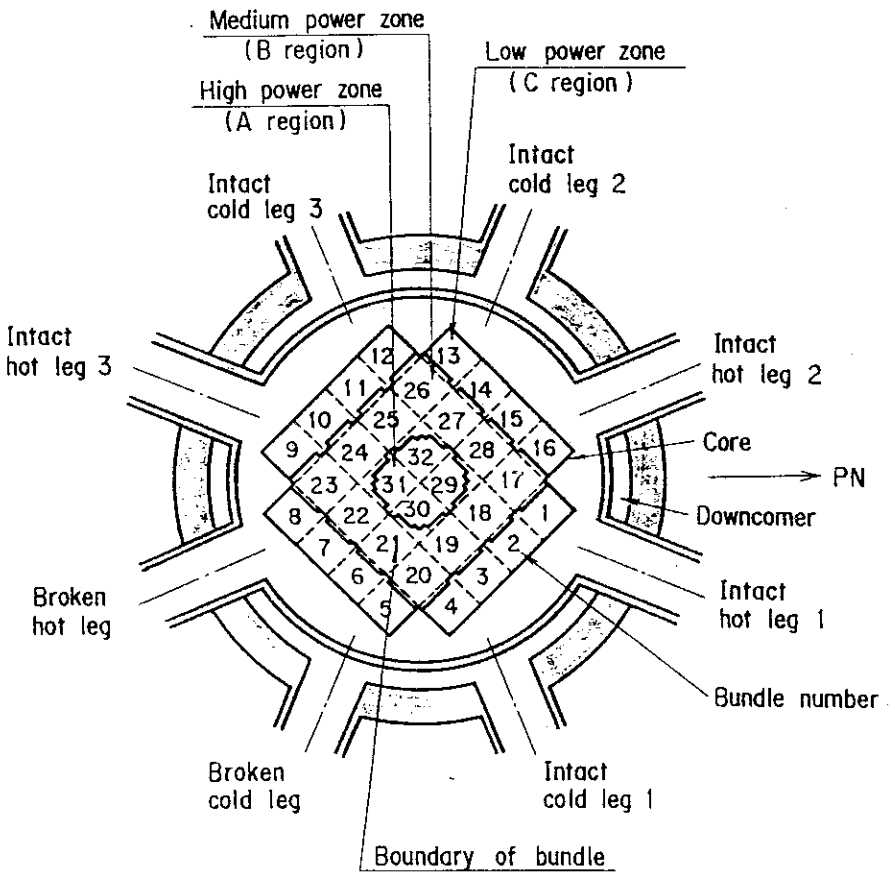

Fig. A-1 Definition of power zones and bundle numbers

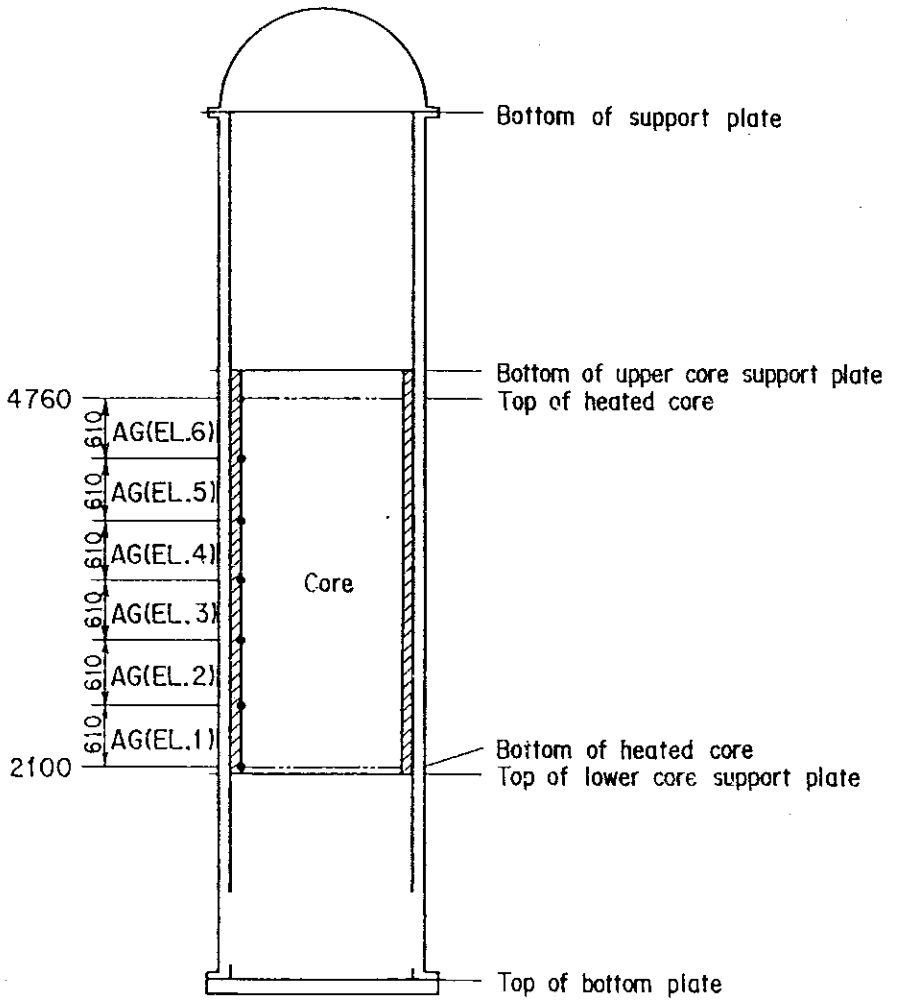

Fig. A-2 Definition of Tag.ID for void fraction
(AG(EL.1) ∿ AG(EL.6))

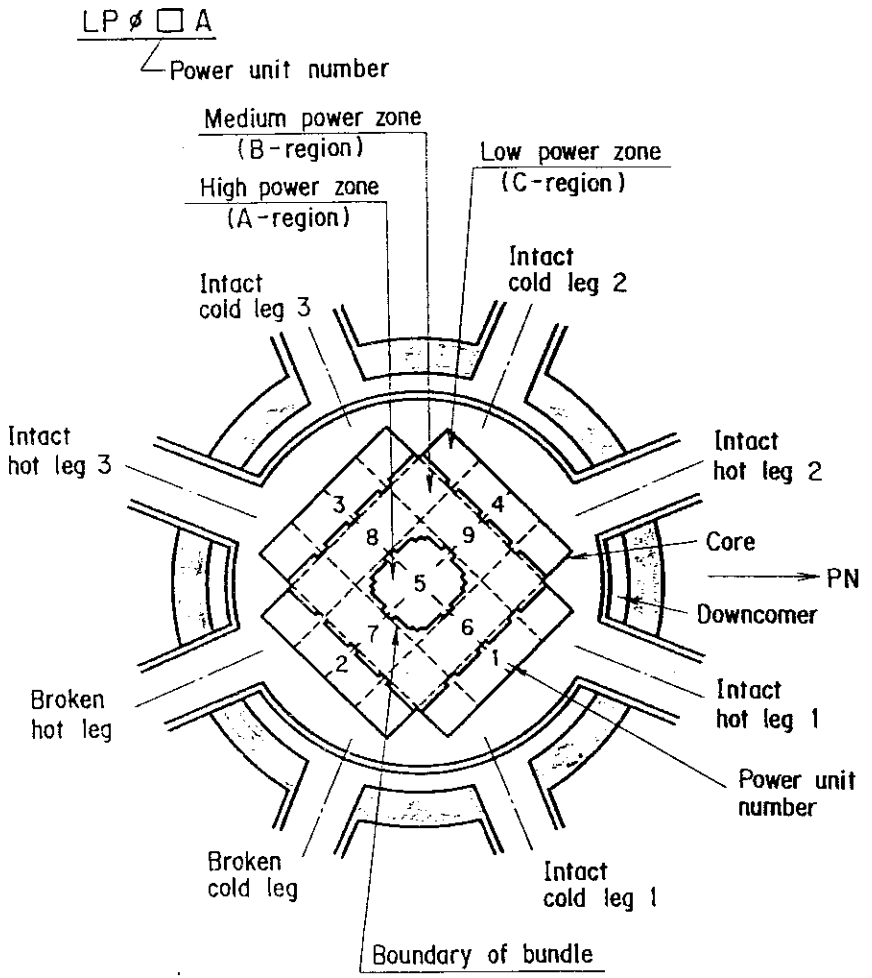

Fig. A-3 Definition of Tag.ID for average linear power of heater rod in each power unit zone (LP01A ∿ LP09A)

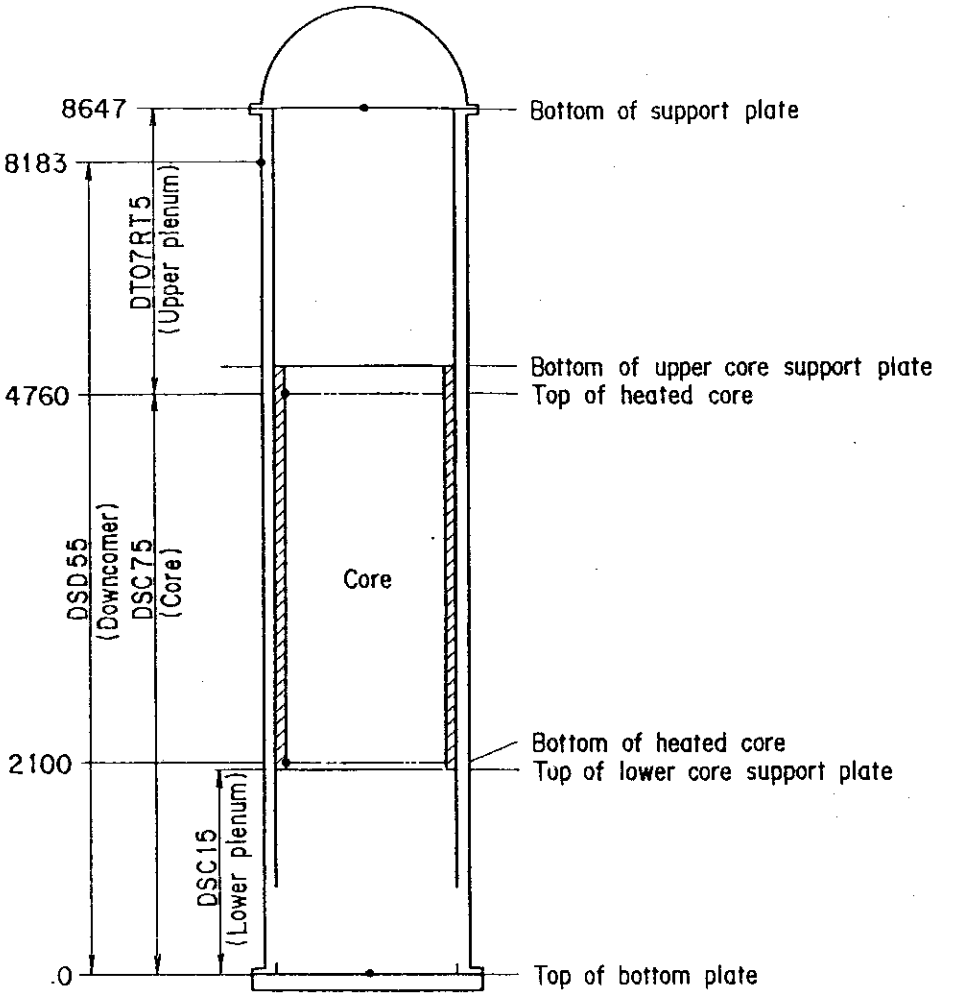

Fig. A-4 Definition of Tag.ID for differential pressure through downcomer, upper plenum, core, and lower plenum (DSD55, DTO7RT5, DSC75, DSC15)

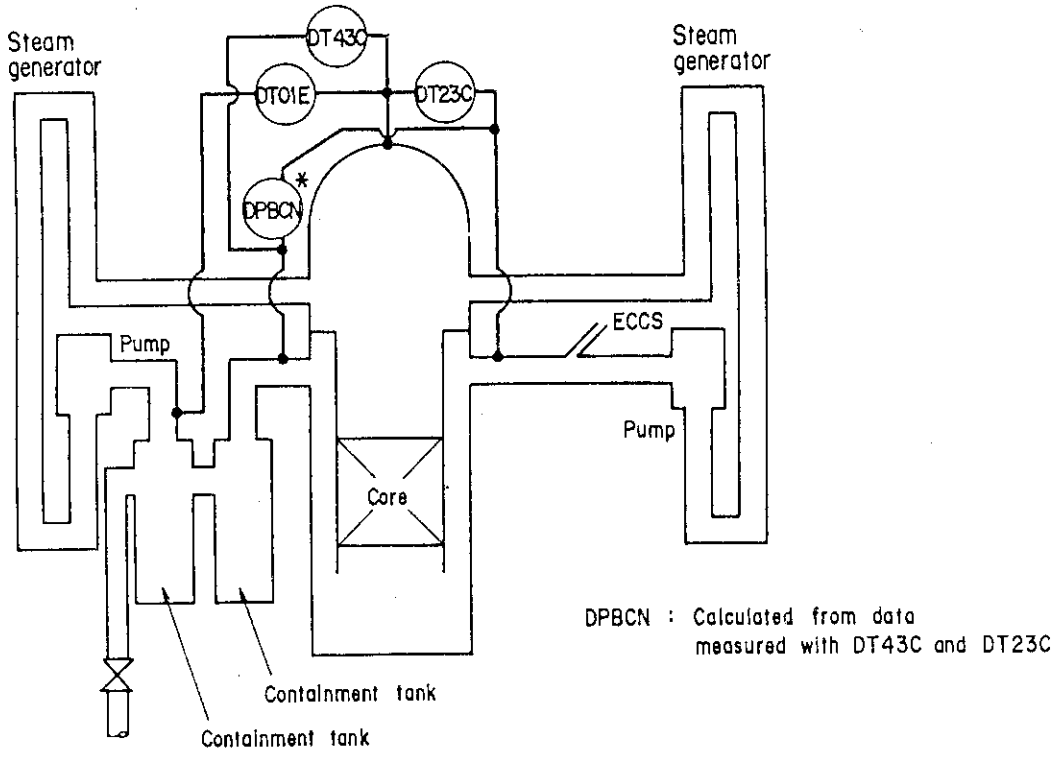

Fig. A-5 Definition of Tag.ID for differential pressure through intact and broken loop and broken cold leg nozzle (DT23C, DT01B, DPBCN)

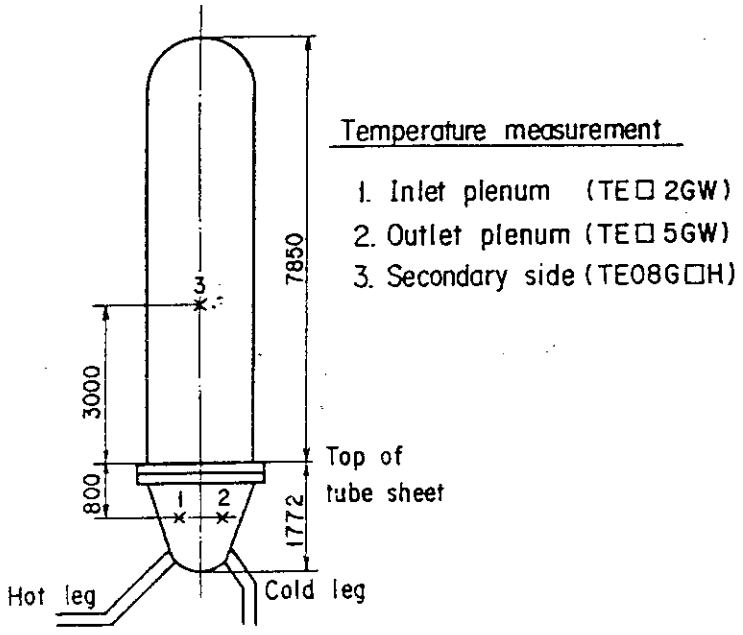

Fig. A-6 Definition of Tag.ID for fluid temperature in inlet and outlet plenum and secondary of steam generator (TE□2GW, TE□5GW, TE08G□H)

Appendix B

Main results of Test C1-1 (Run 10)

Table and Figure List

Table B-1 Summary of test conditions

1. TEST TYPE : TEST C1-1 (CCTF MAIN TEST NO.1)
2. TEST NUMBER : RUN 010 3. DATE : JUNE 21, 1979
4. POWER : A: TOTAL: 9.35 MW; B:LINEAR: 1.4 KW/M
5. RELATIVE RADIAL POWER SHAPE :

   A: ZONE: A B C

   B: RATIO: 1.08 1.0 0.82
6. AXIAL POWER SHAPE : CHOPPED COSINE
7. PRESSURE (KG/CM^2A) :

   A: SYSTEM: 2.07, B: CONTAINMENT 2.07,

   C: STEAM GENERATOR SECONDARY: 50
8. TEMPERATURE (DEG.C) :

   A: DOWNCOMER WALLS 188, B: VESSEL INTERNALS 117

   C: PRIMARY PIPING WALLS 122, D: LOWER PLENUM LIQUID 116

   E: ECC LIQUID 35 ,F: STEAM GENERATOR SECONDARY 263

   G: CORE TEMPERATURE AT ECC INITIATION 506
9. ECC INJECTION TYPE: C

   A: COLD LEG, B: LOWER PLENUM, C: LOWER PLENUM + COLD LEG
10. PUMP K-FACTOR : ∿25 (UNCERTAIN)
11. ECC FLOW RATES AND DURATION :

    A: ACCUMULATOR 264 M^3/HR FROM 0 TO 21 SECONDS

    B: LPCI 30.6 M^3/HR FROM 21 TO 705.5 SECONDS

    C: ECC INJECTION TO LOWER PLENUM : FROM 0 TO 15.5 SECONDS

    (VALVE OPENING AND CLOSING TIMES ARE INCLUDED IN THE INJECTION DURATION)
12. INITIAL WATER LEVEL IN LOWER PLENUM : 0.87 M.
13. POWER CONTROL : ANS x 1.2 + ACTINIDE (30 SEC AFTER SCRAM)
14. EXPECTED BOCREC TIME FROM ECC INITIATION 12 SEC
15. EXPECTED PEAK TEMPERATURE AT BOCREC 600 C

Table B-2 Chronology of events

EVENT	TIME (sec)
Test initiated (Heater rods power on) (Data recording initiated)	0.0
Accumulator injection initiated	54
Power decay initiated (Bottom of core recovery)	66
Accumulator injection switched from lower plenum to cold leg	69.5
Accumulator injection ended and LPCI injection initiated	75
All heater rods quenched	633
Power off	664
LPCI injection ended	759.5
Test ended (Data recording ended)	1073

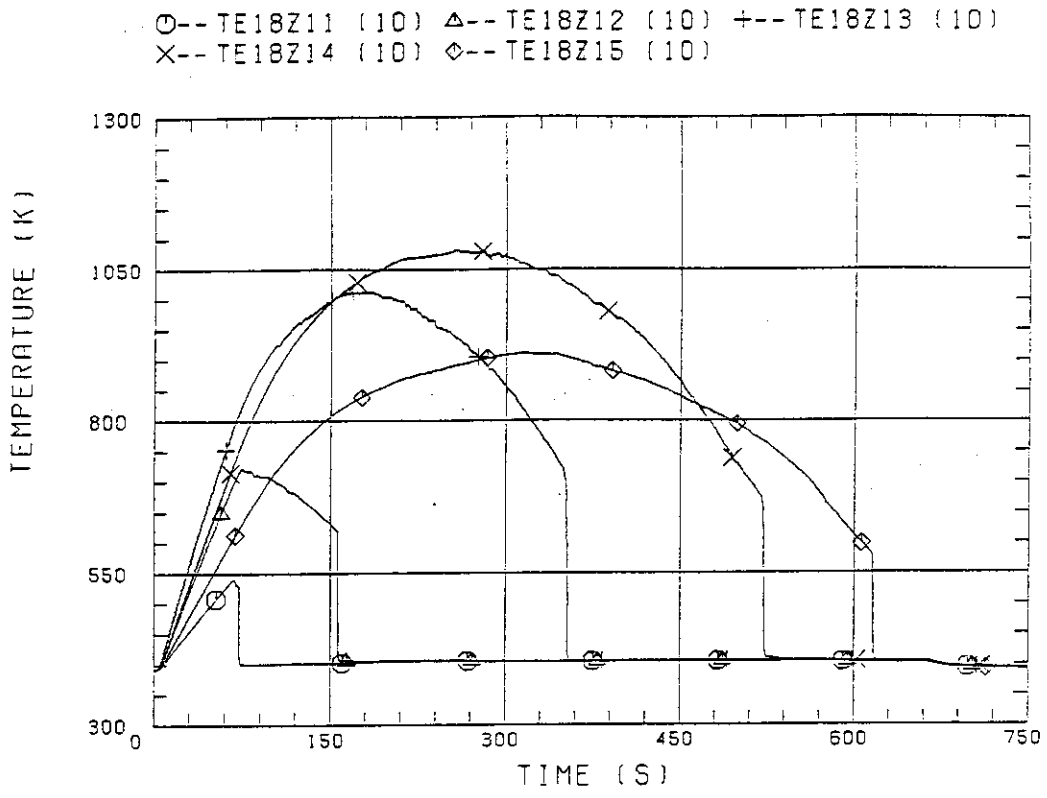

Fig. B-1 Surface temperature on low power rod (Z-rod) in medium power region (B region) (average power rod)

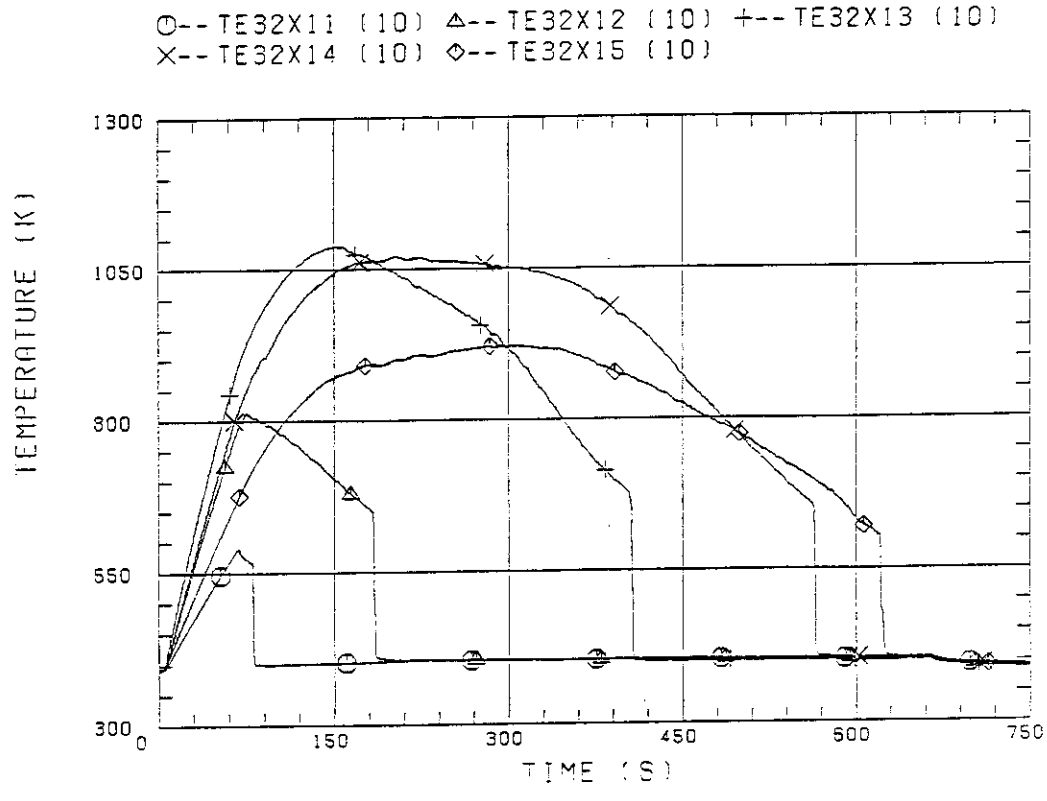

Fig. B-2 Surface temperature on high power rod (X-rod) in high power region (A region) (peak power rod)

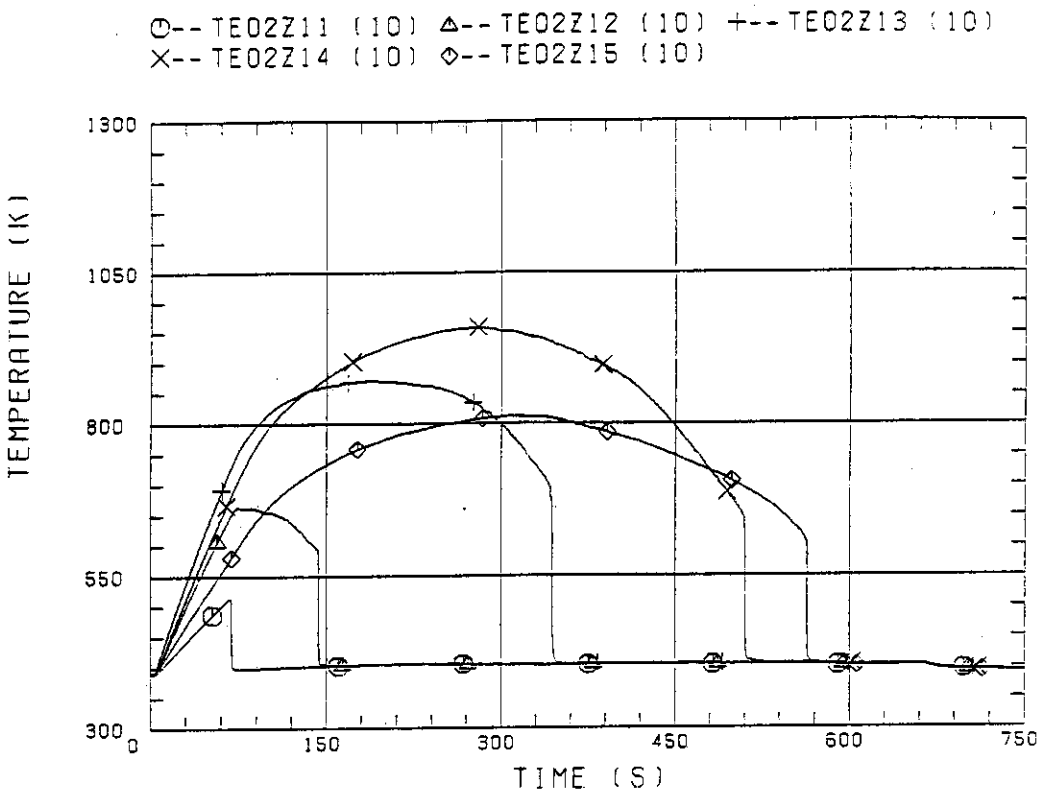

Fig. B-3 Surface temperature on low power rod (Z-rod) in low power region (C region) (lowest power rod)

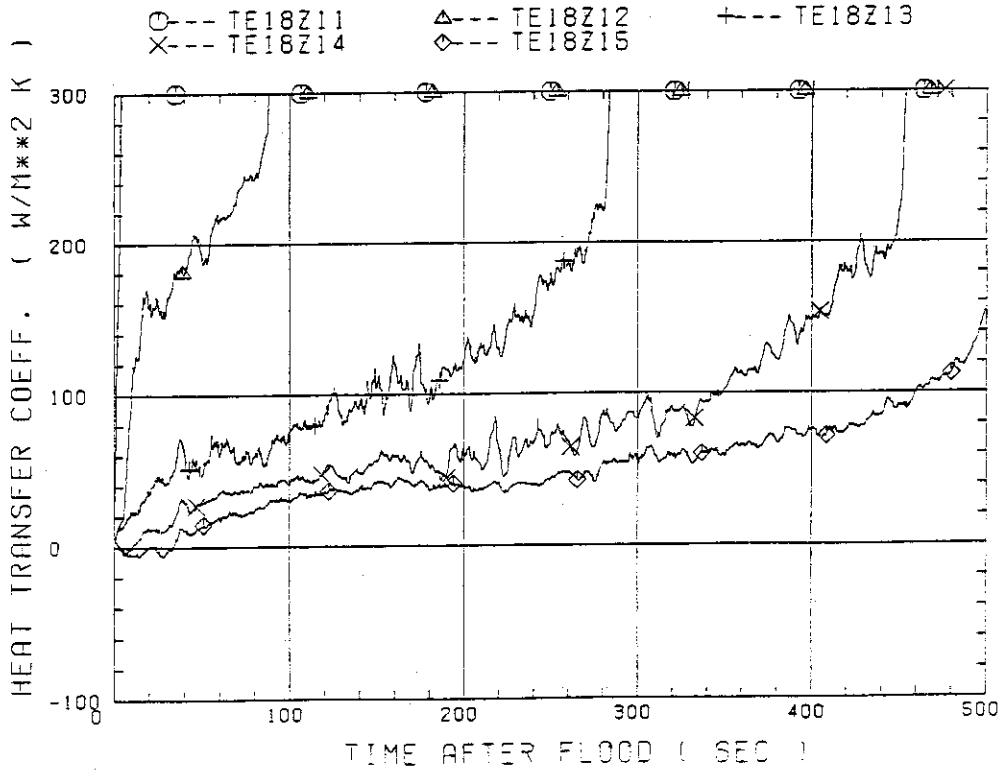

Fig. B-4 Heat transfer coefficient at midplane of low power rod (Z-rod) in medium power region (B region) (average power rod)

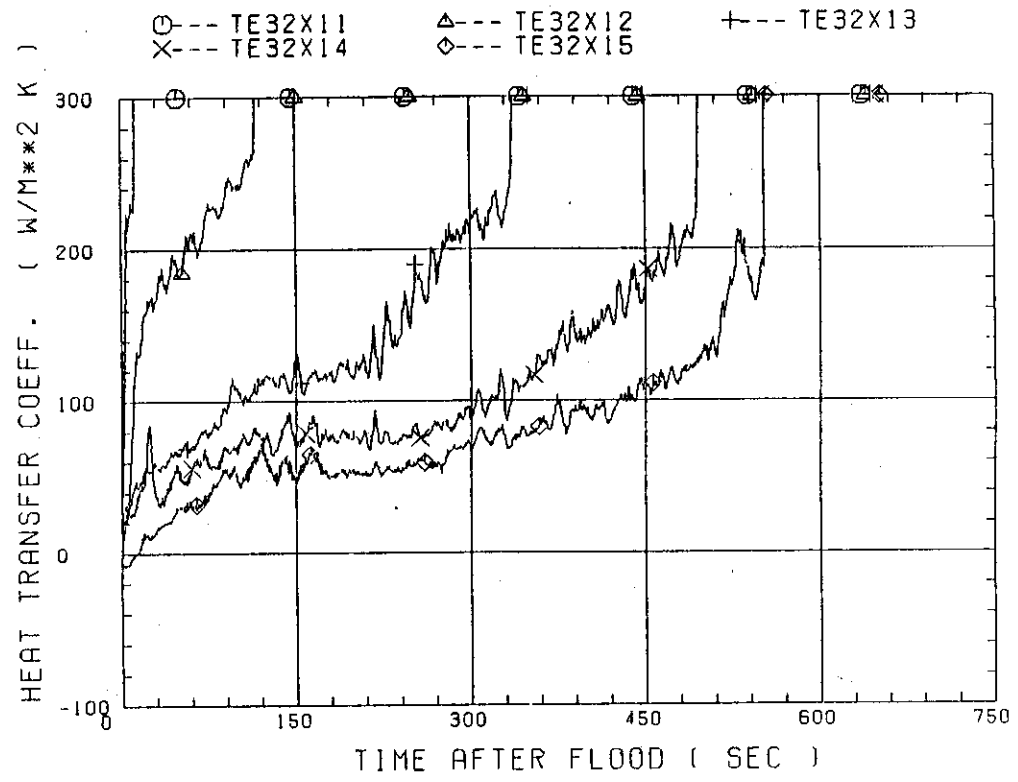

Fig. B-5 Heat transfer coefficient at midplane of high power rod (X-rod) in high power region (A region) (peak power rod)

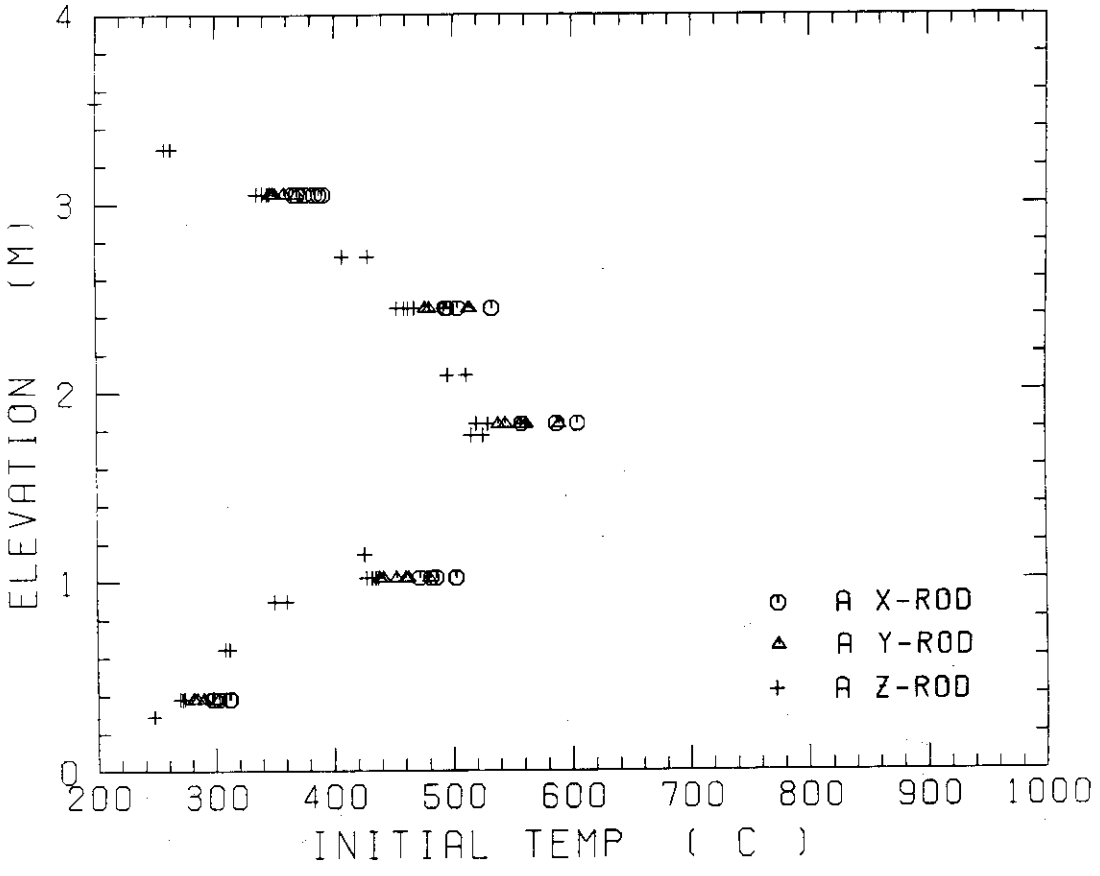

Fig. B-6 Initial rod surface temperature in high power region (A region)

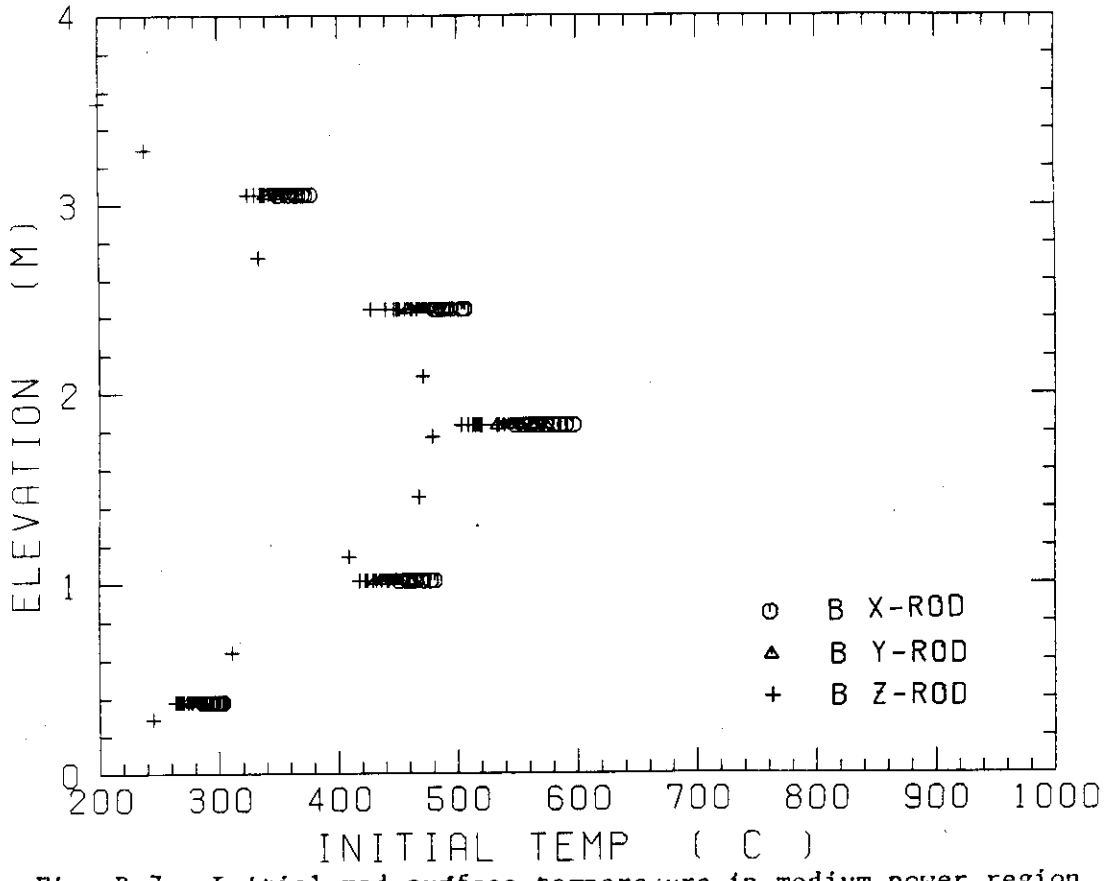

Fig. B-7 Initial rod surface temperature in medium power region (B region)

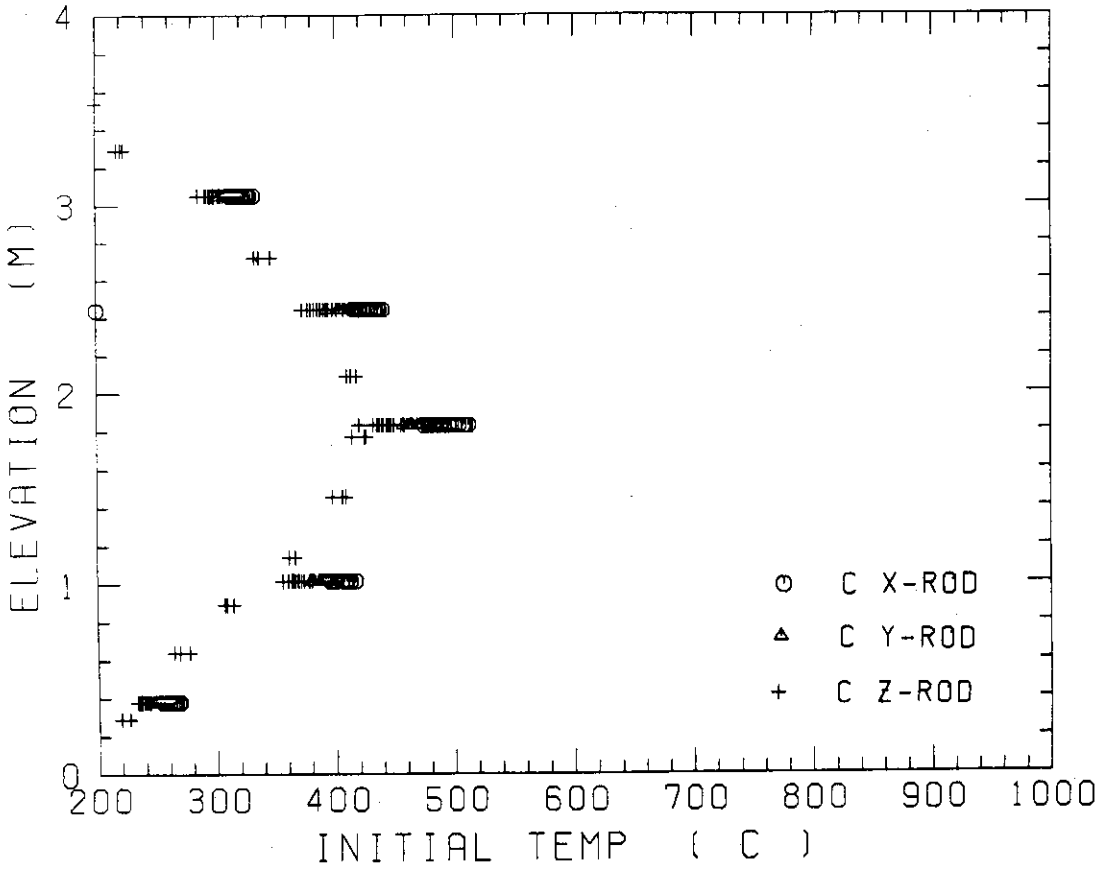

Fig. B-8 Inital rod surface temperature in low power region (C region)

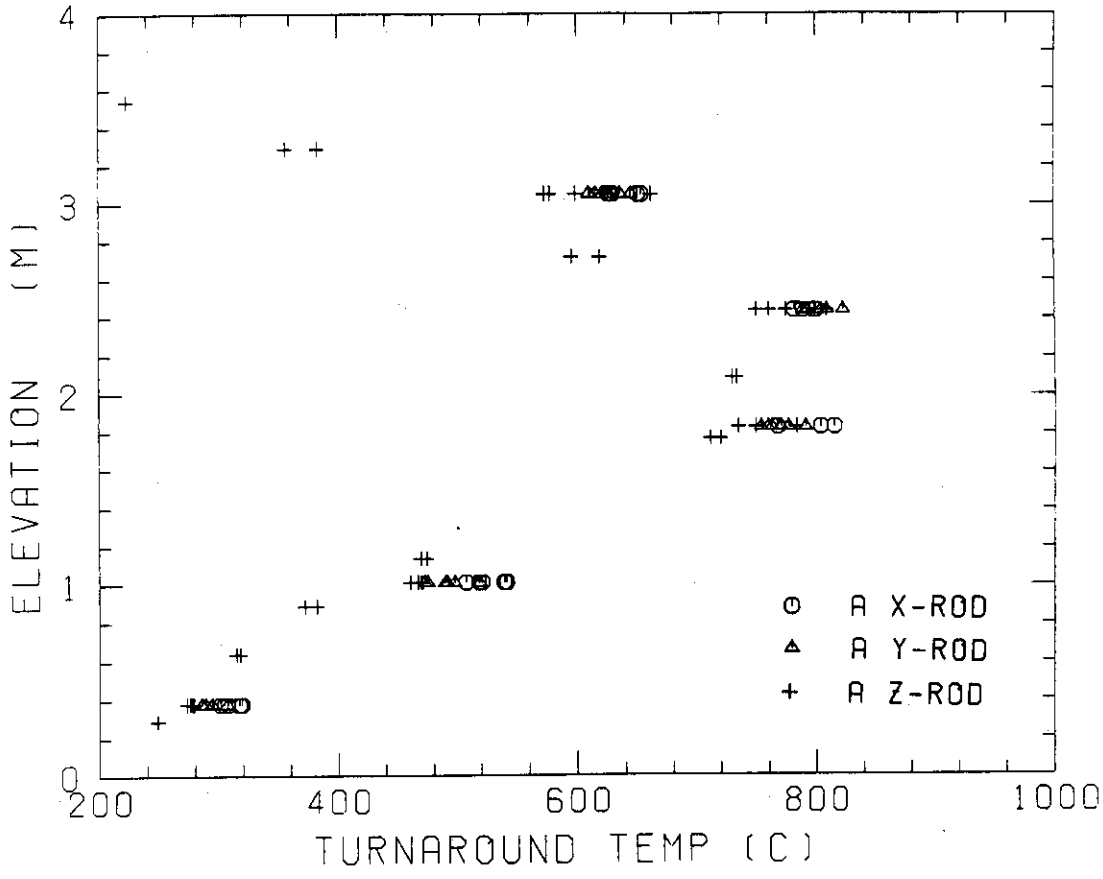

Fig. B-9 Turnaround temperature in high power region (A region)

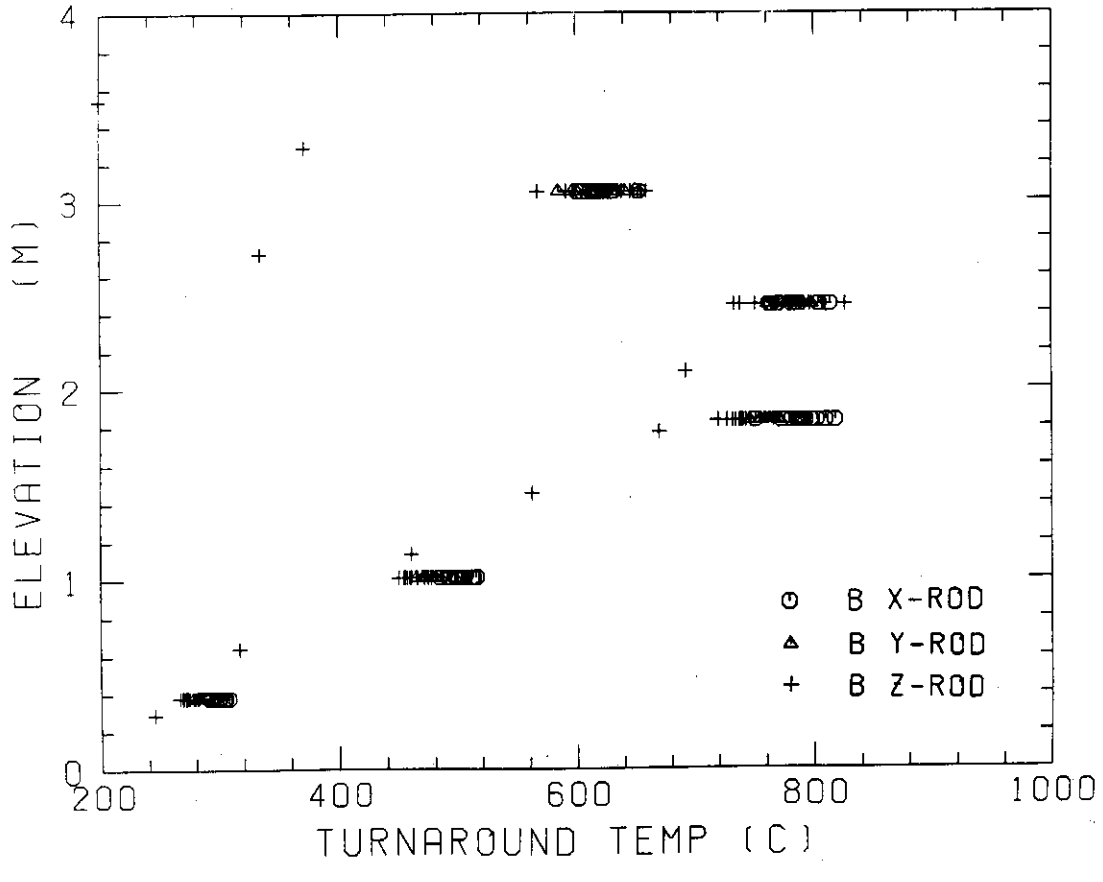

Fig. B-10 Turnaround temperature in medium power region (B region)

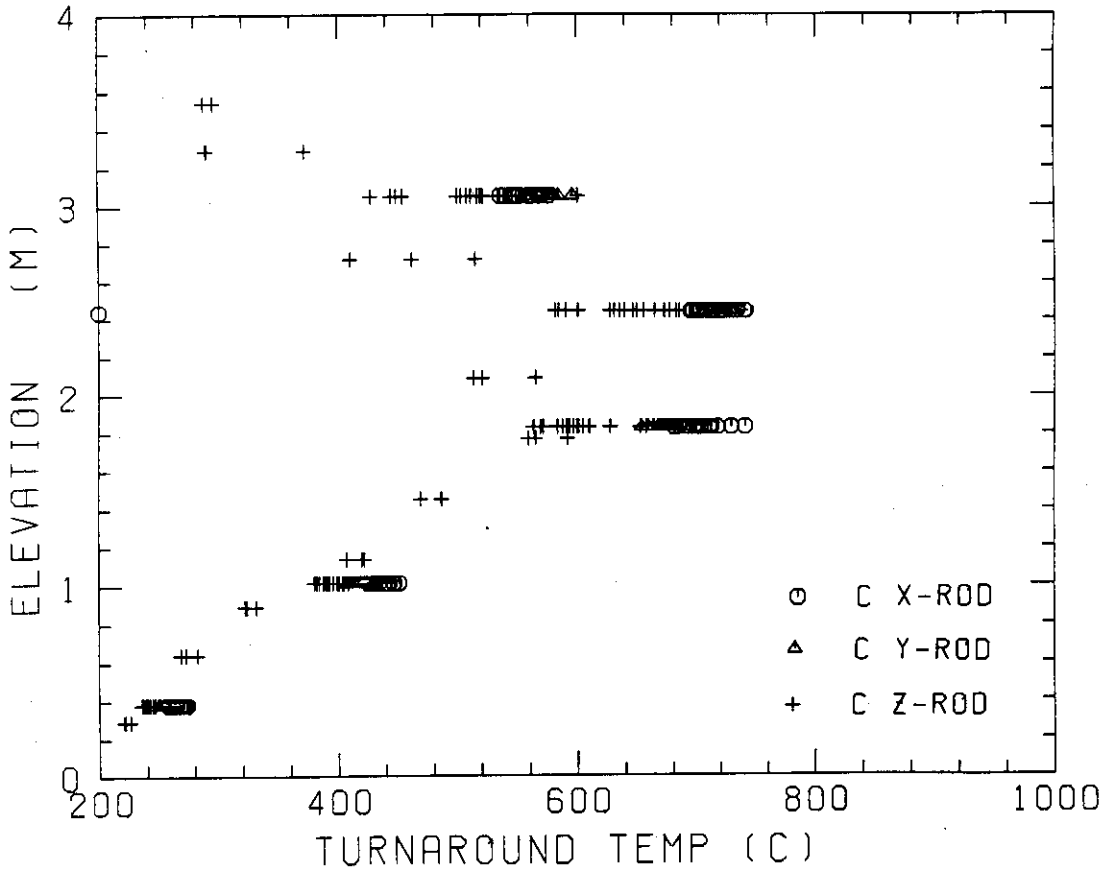

Fig. B-11 Turnaround temperature in low power region (C region)

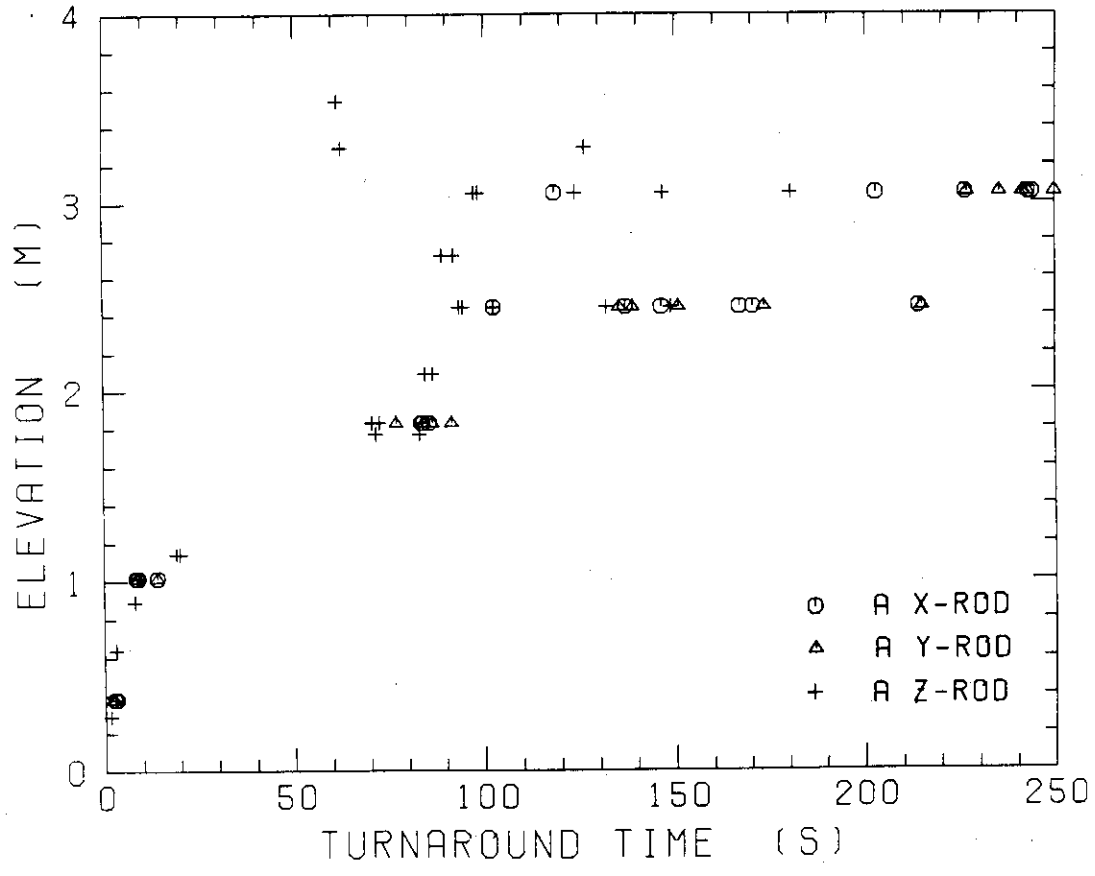

Fig. B-12 Turnaround time in high power region (A region)

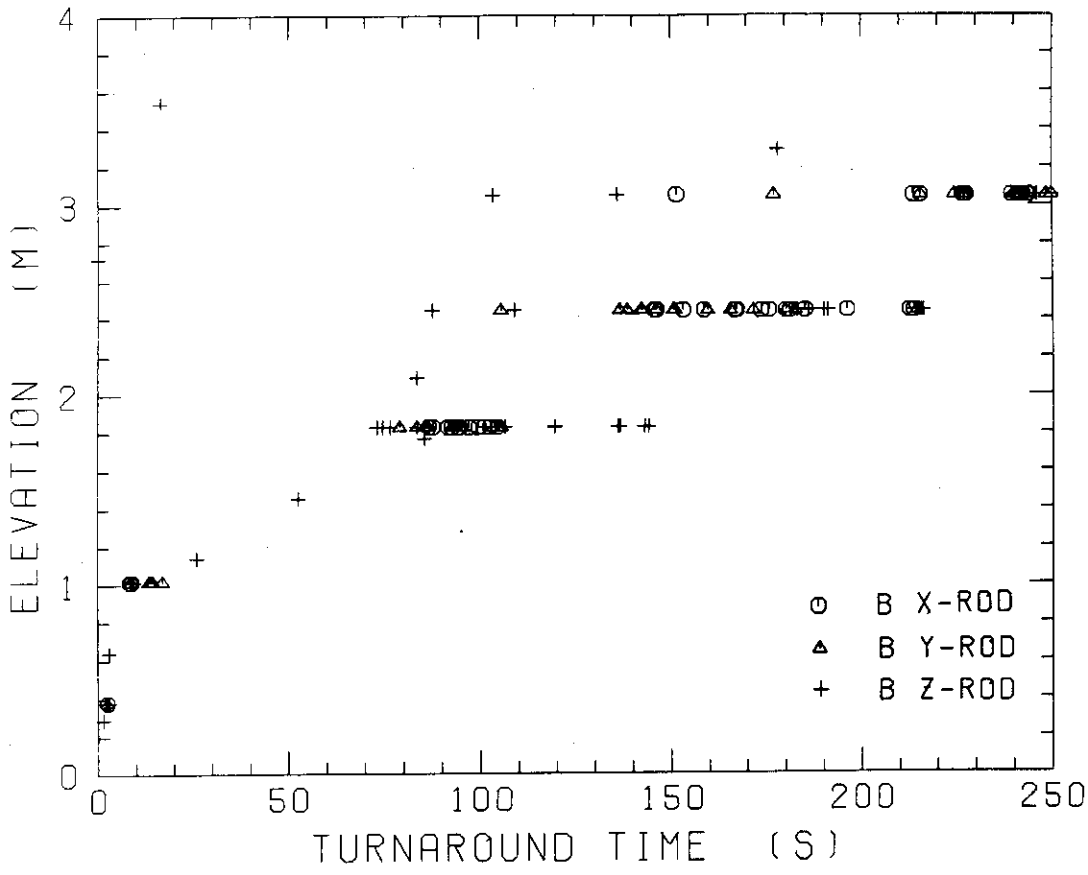

Fig. B-13 Turnaround time in medium power region (B region)

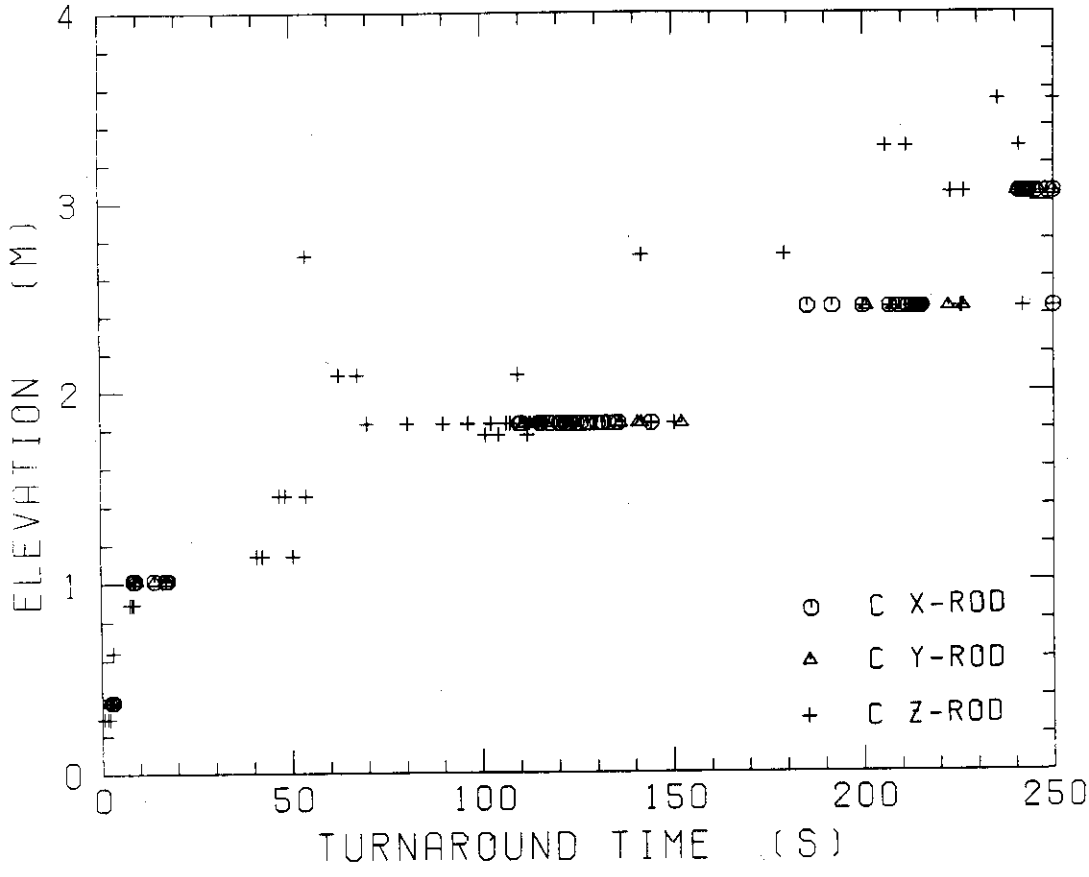

Fig. B-14 Turnaround time in low power region (C region)

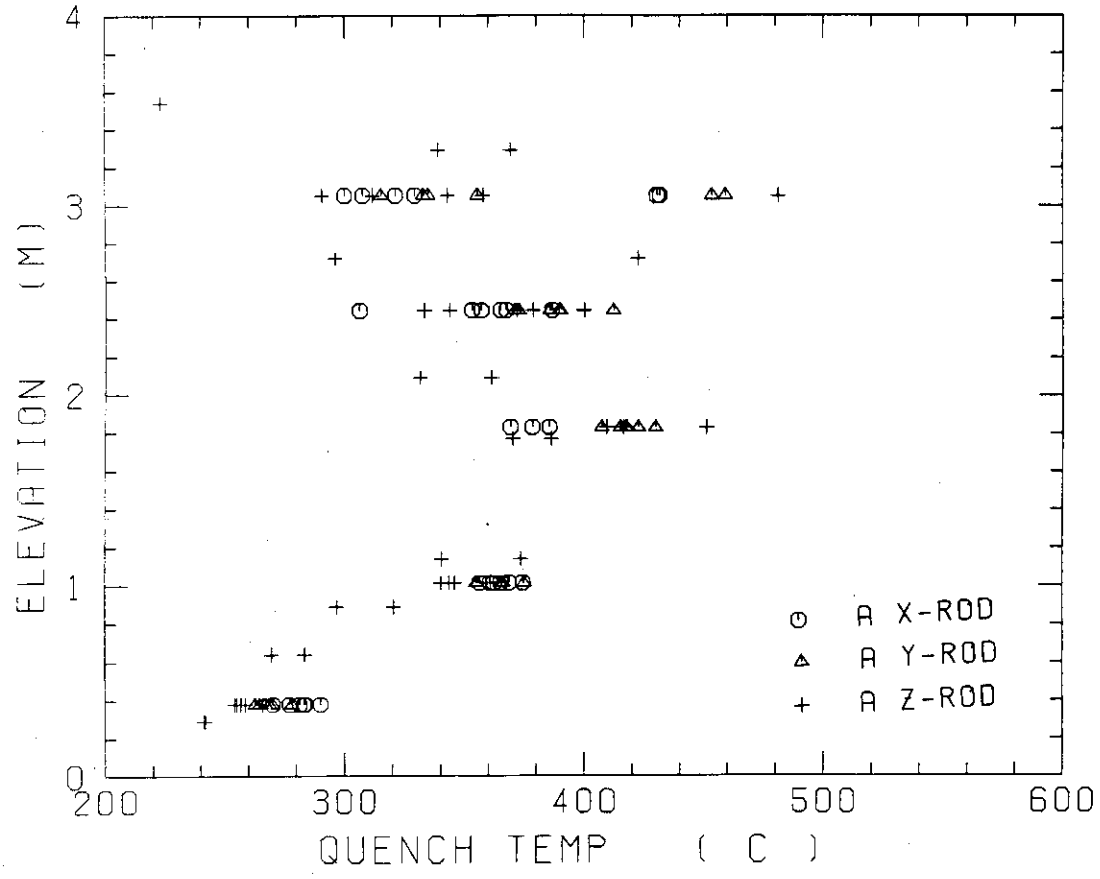

Fig. B-15 Quench temperature in high power region (A region)

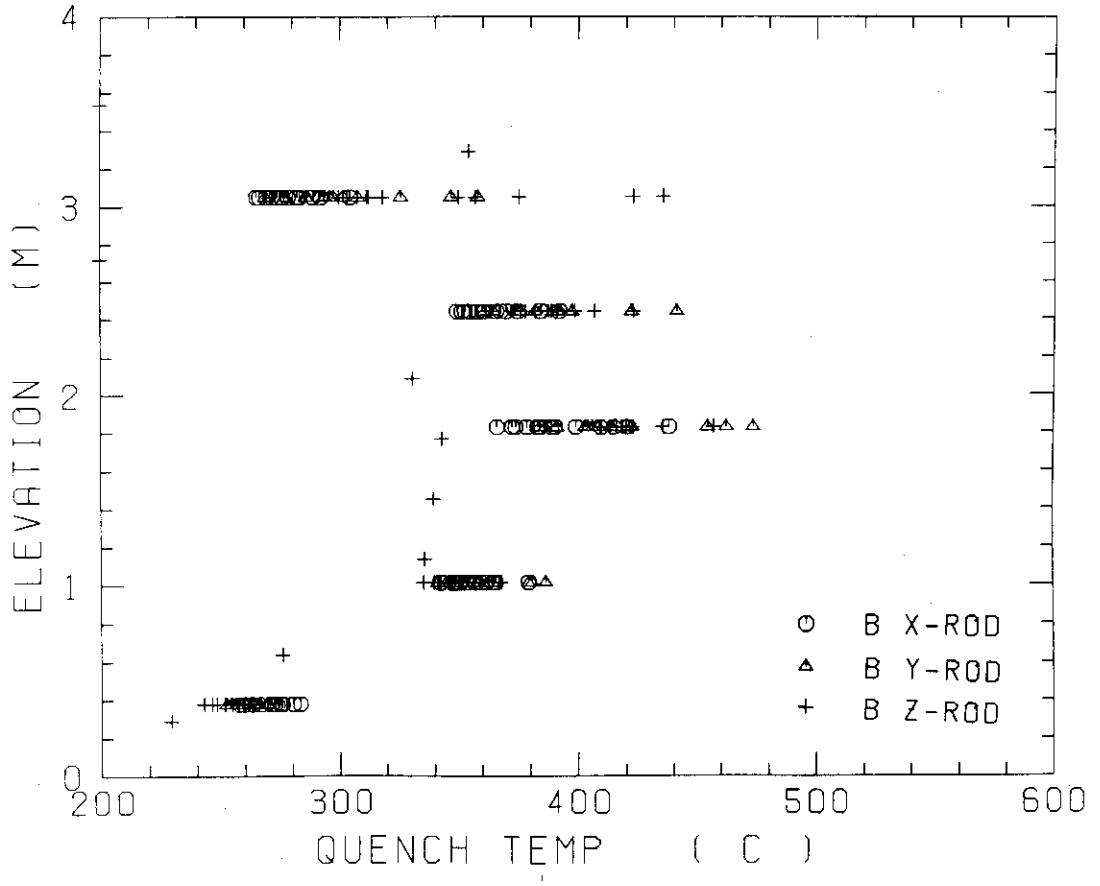

Fig. B-16 Quench temperature in medium power region (B region)

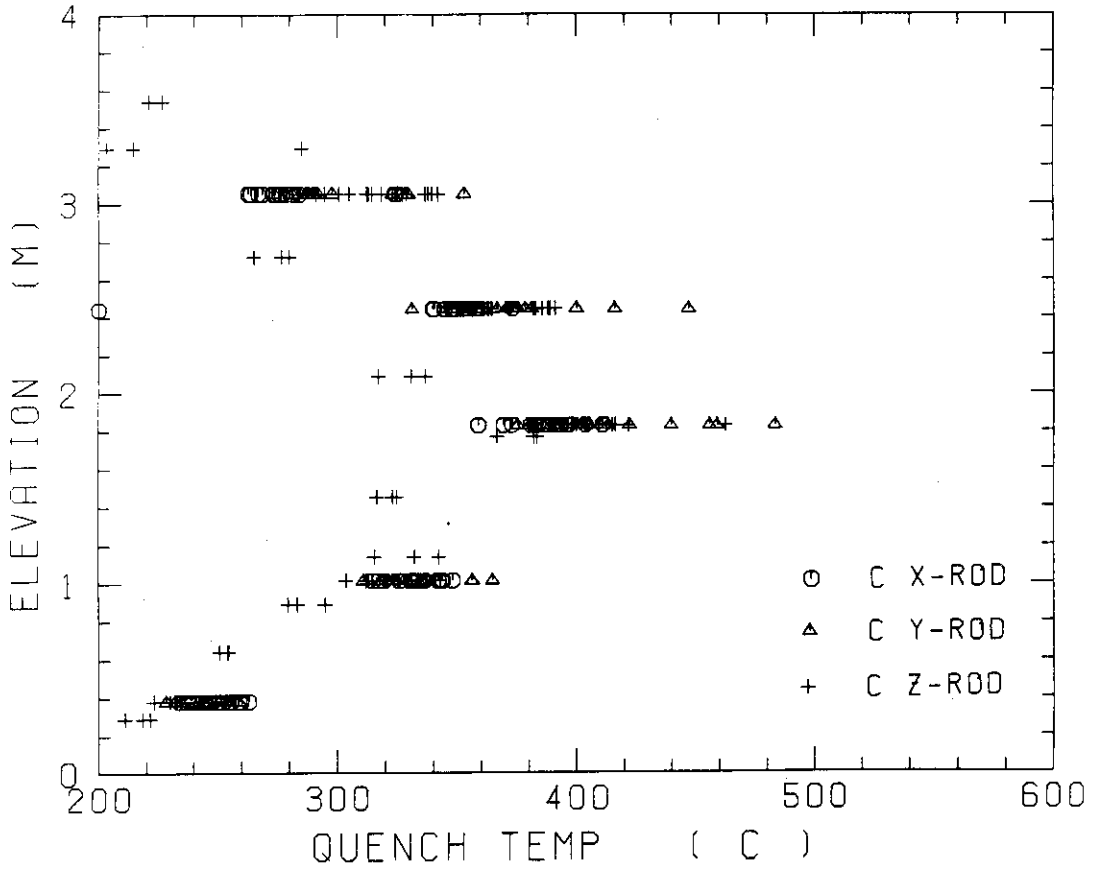

Fig. B-17 Quench temperature in low power region (C region)

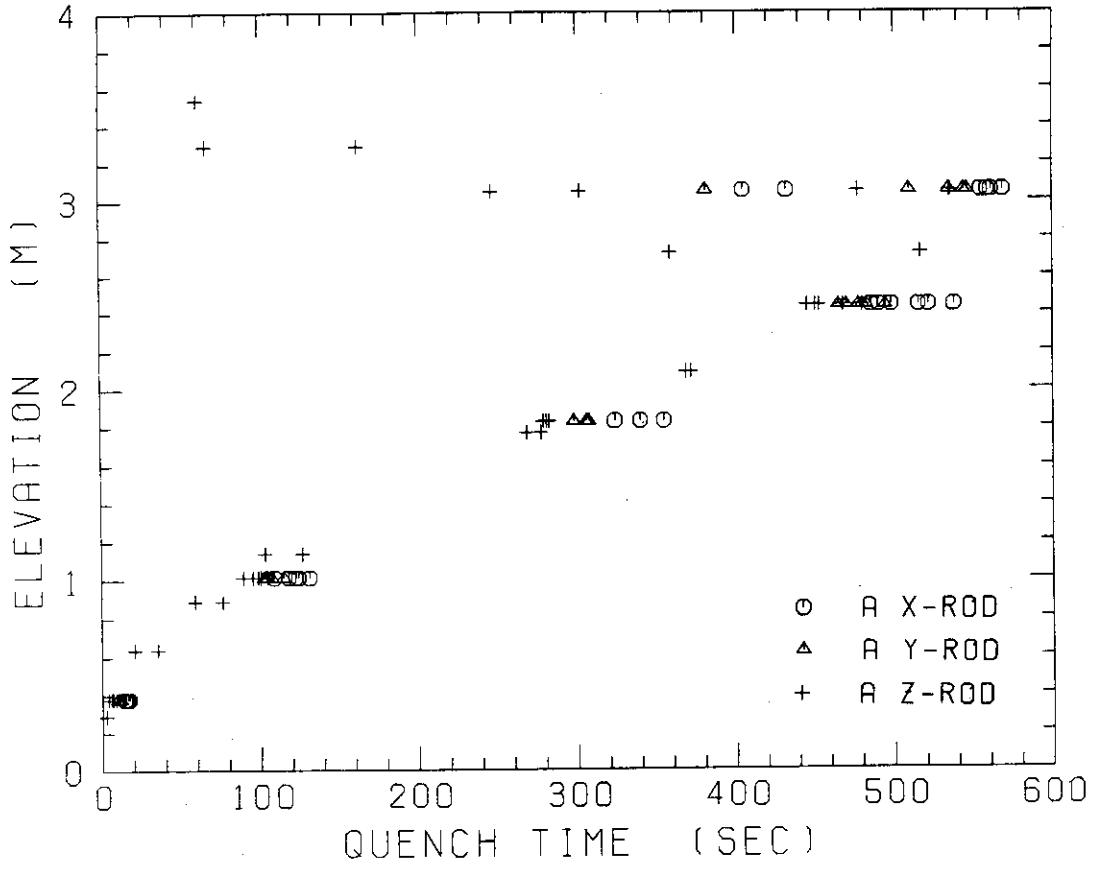

Fig. B-18 Quench time in high power region (A region)

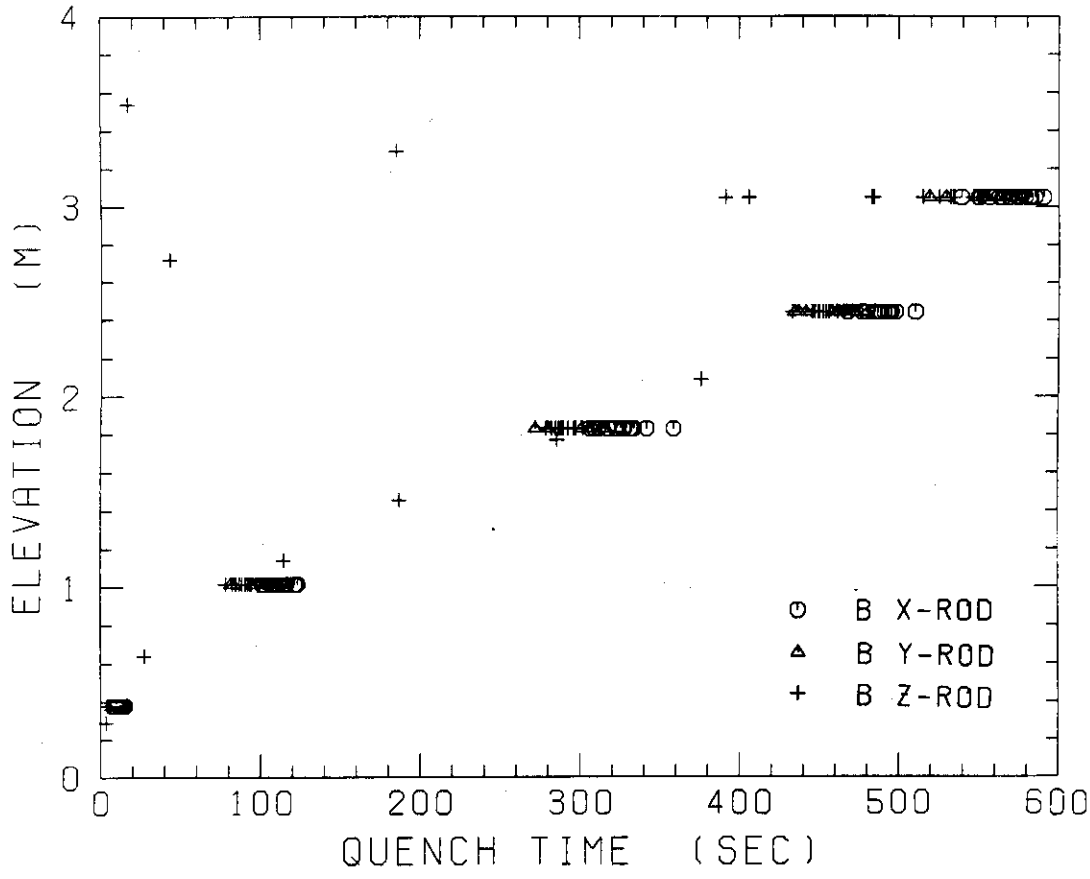

Fig. B-19 Quench time in medium power region (B region)

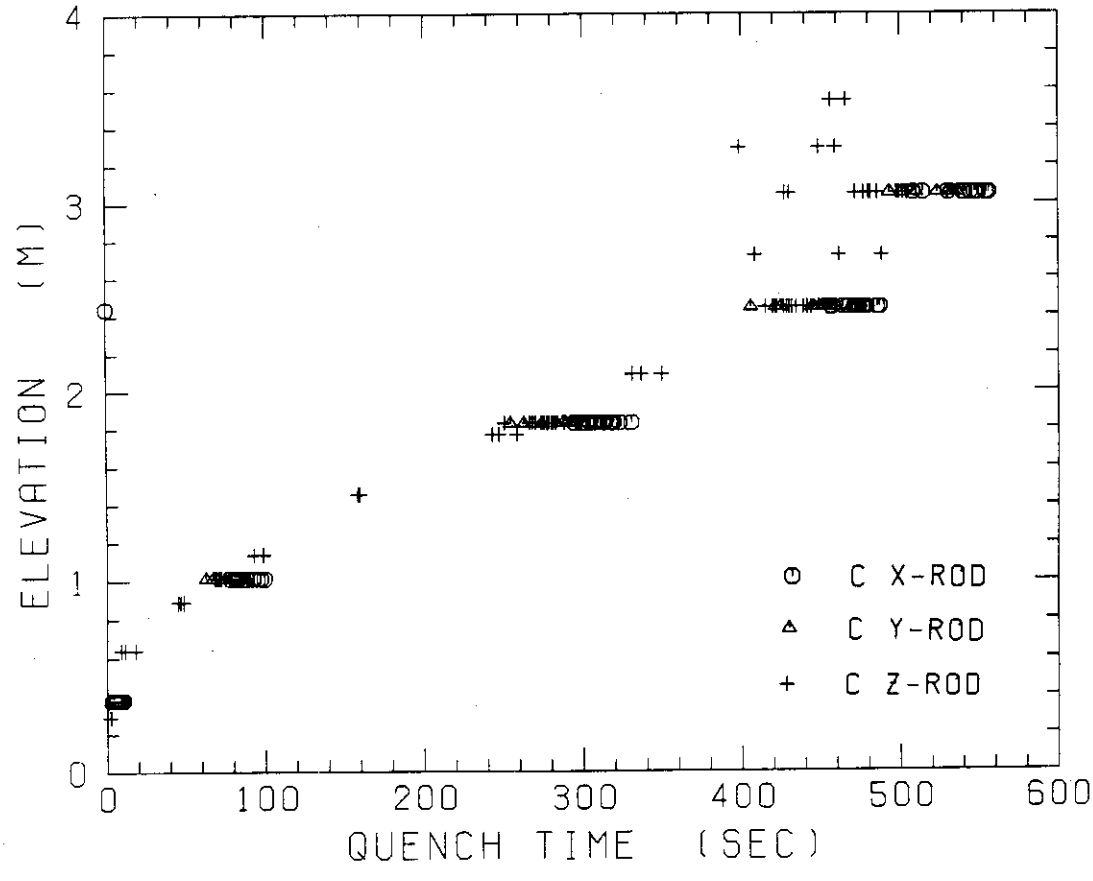

Fig. B-20 Quench time in low power region (C region)

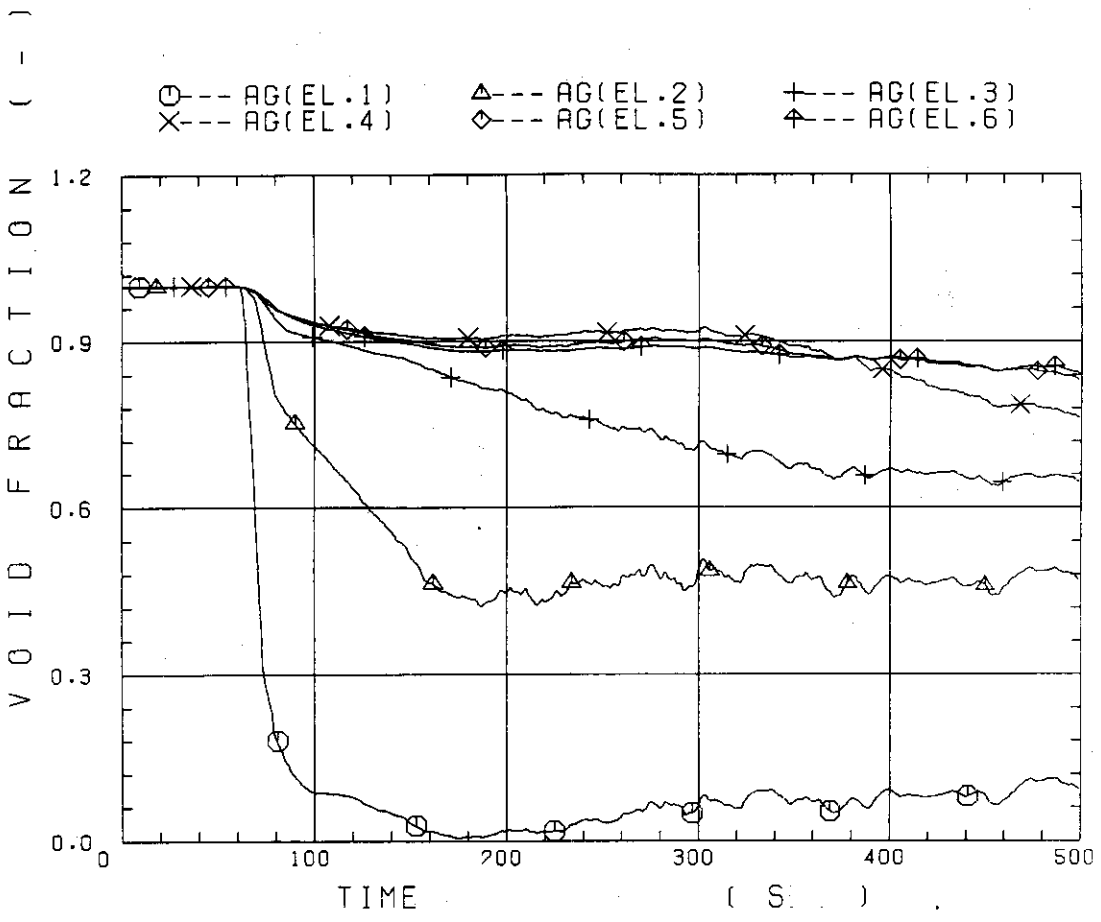

Fig. B-21 Void fraction in core

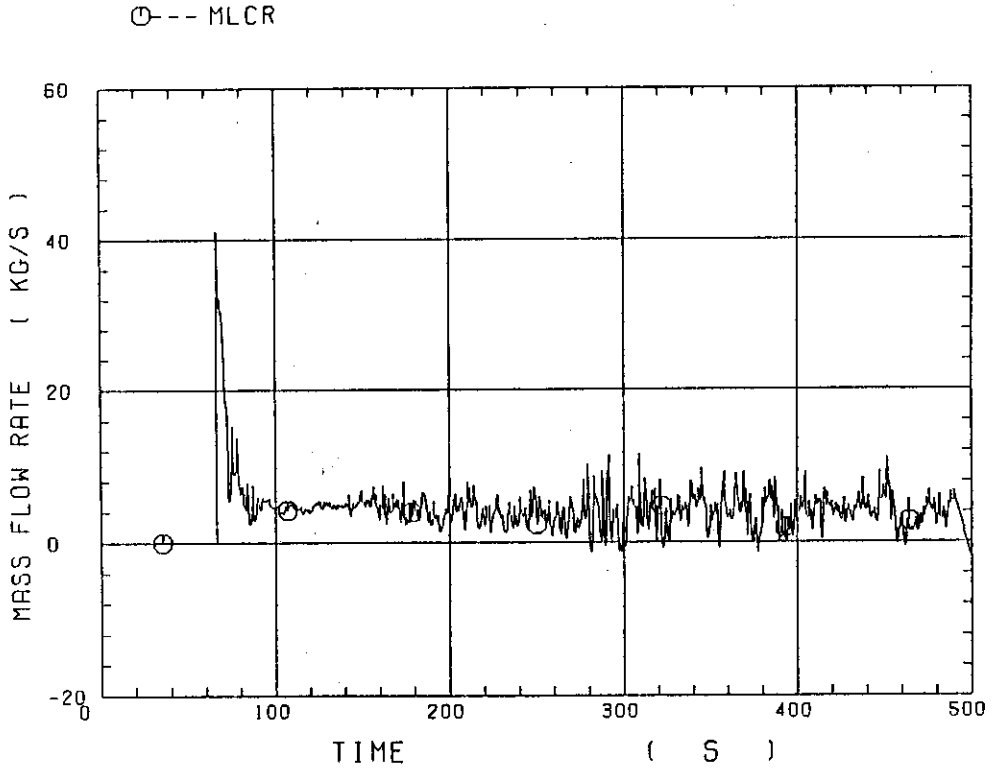

Fig. B-22 Evaluated core inlet mass flow rate

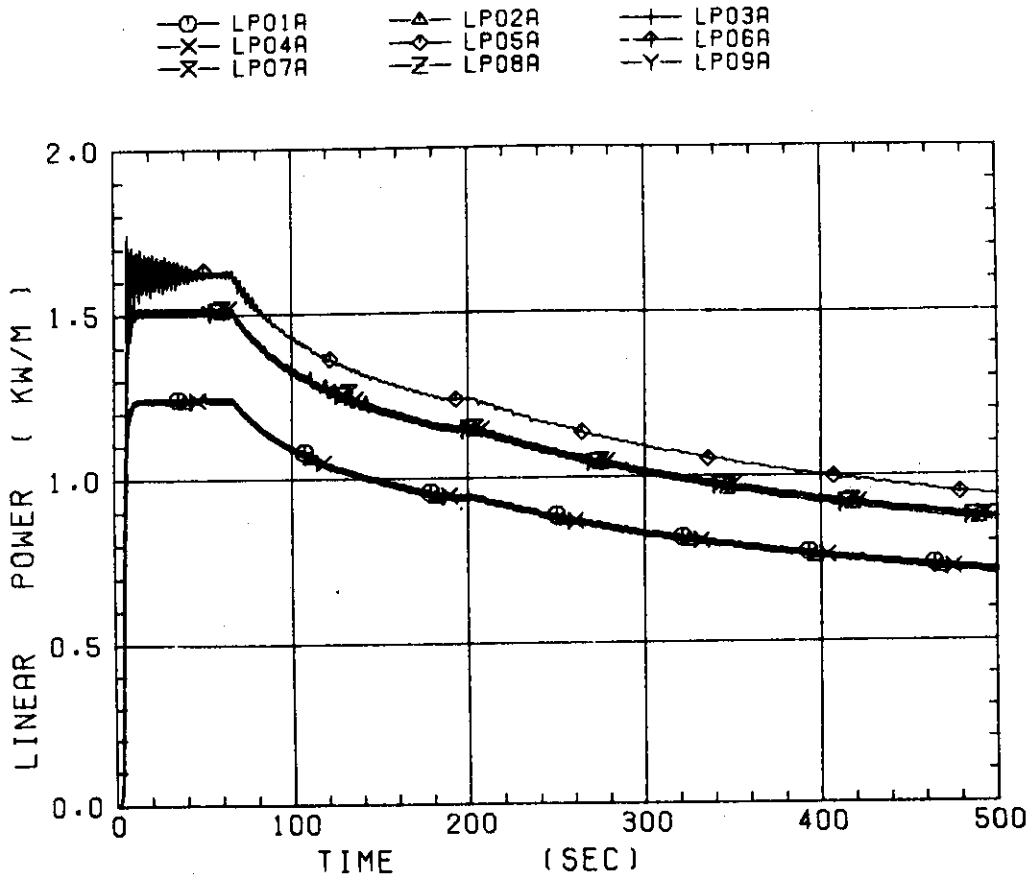

Fig. B-23 Average linear power of heater rod in each power unit zone

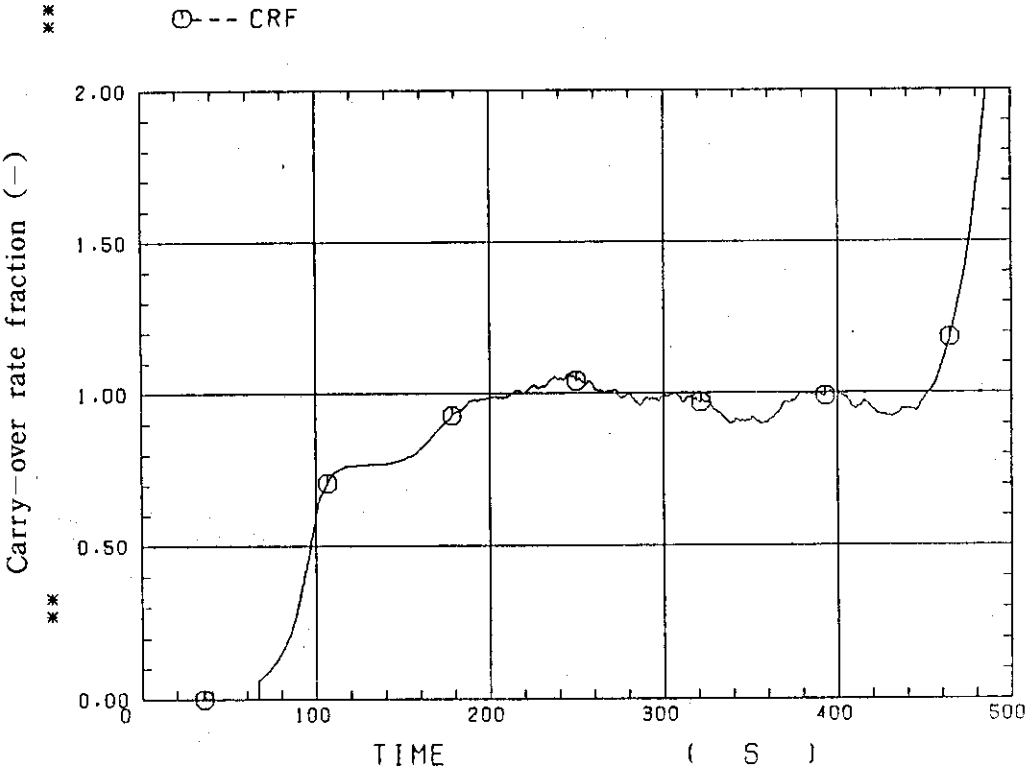

Fig. B-24 Carry-over rate fraction

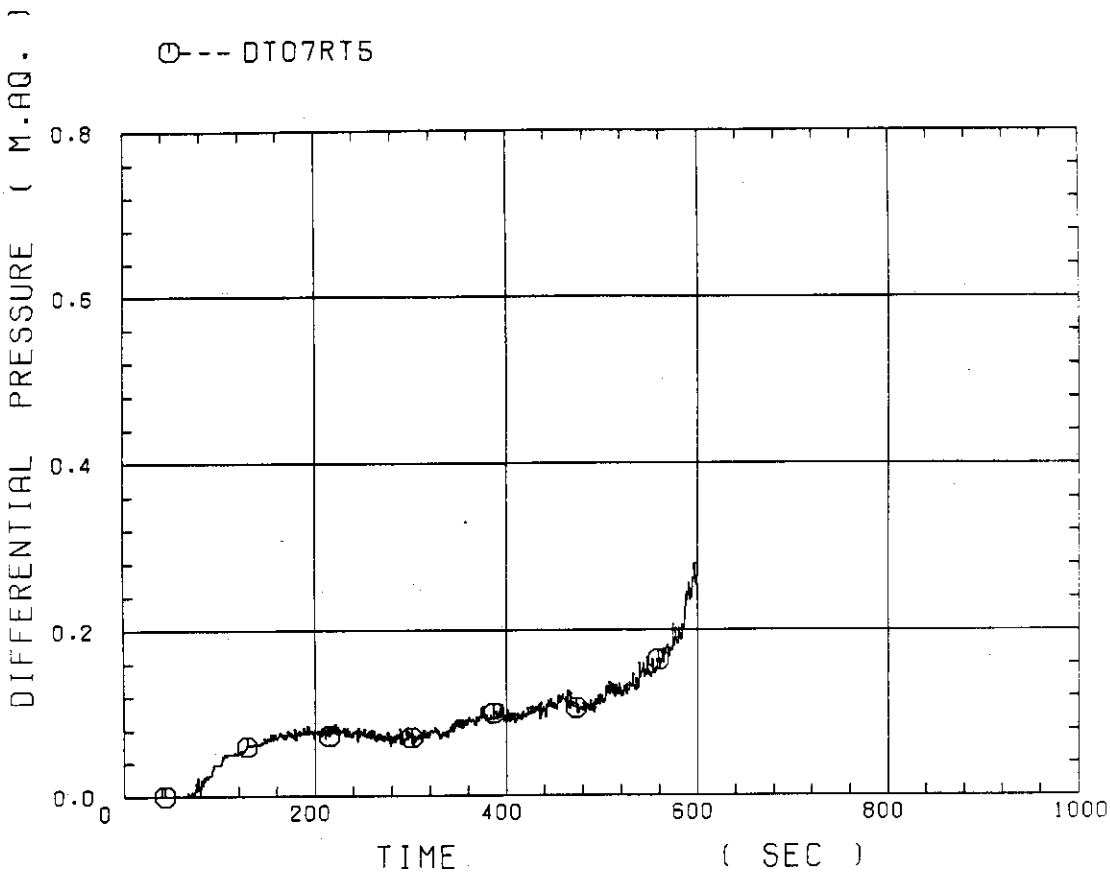

Fig. B-25 Differential pressure through upper plenum

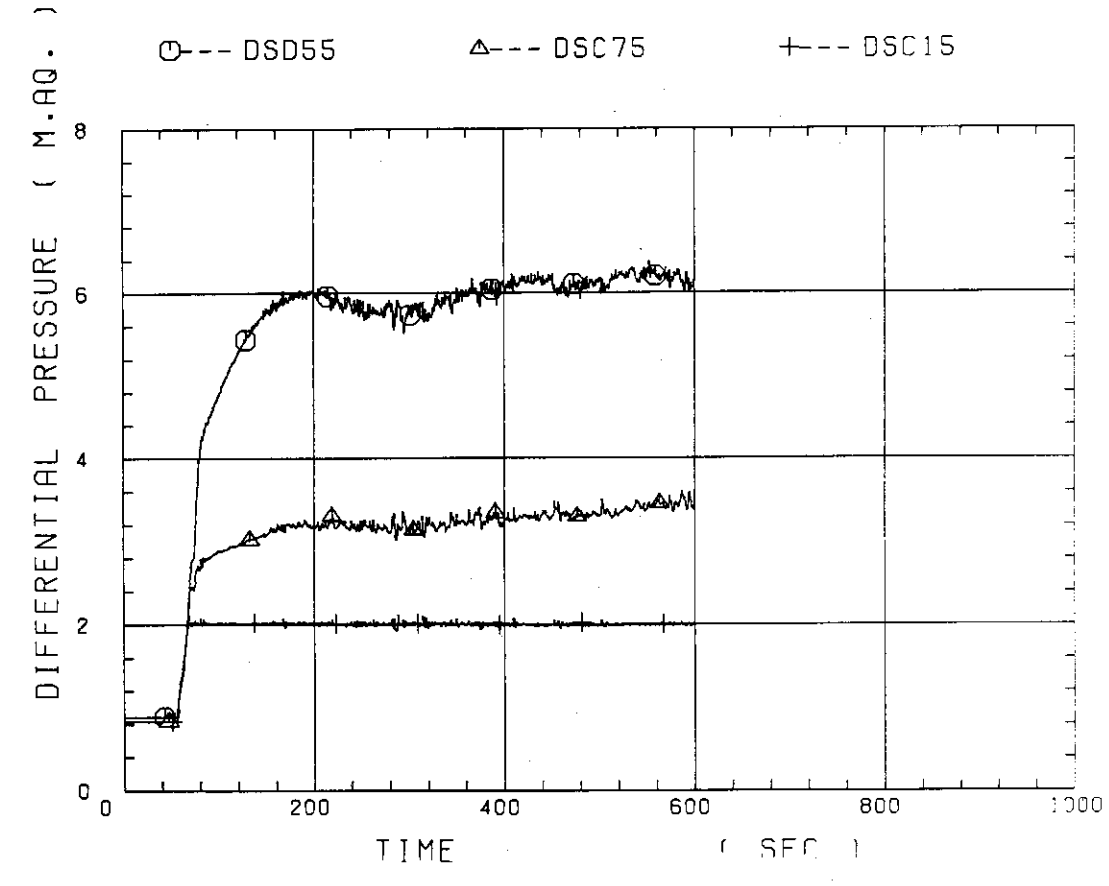

Fig. B-26 Differential pressure through downcomer, core, and lower plenum

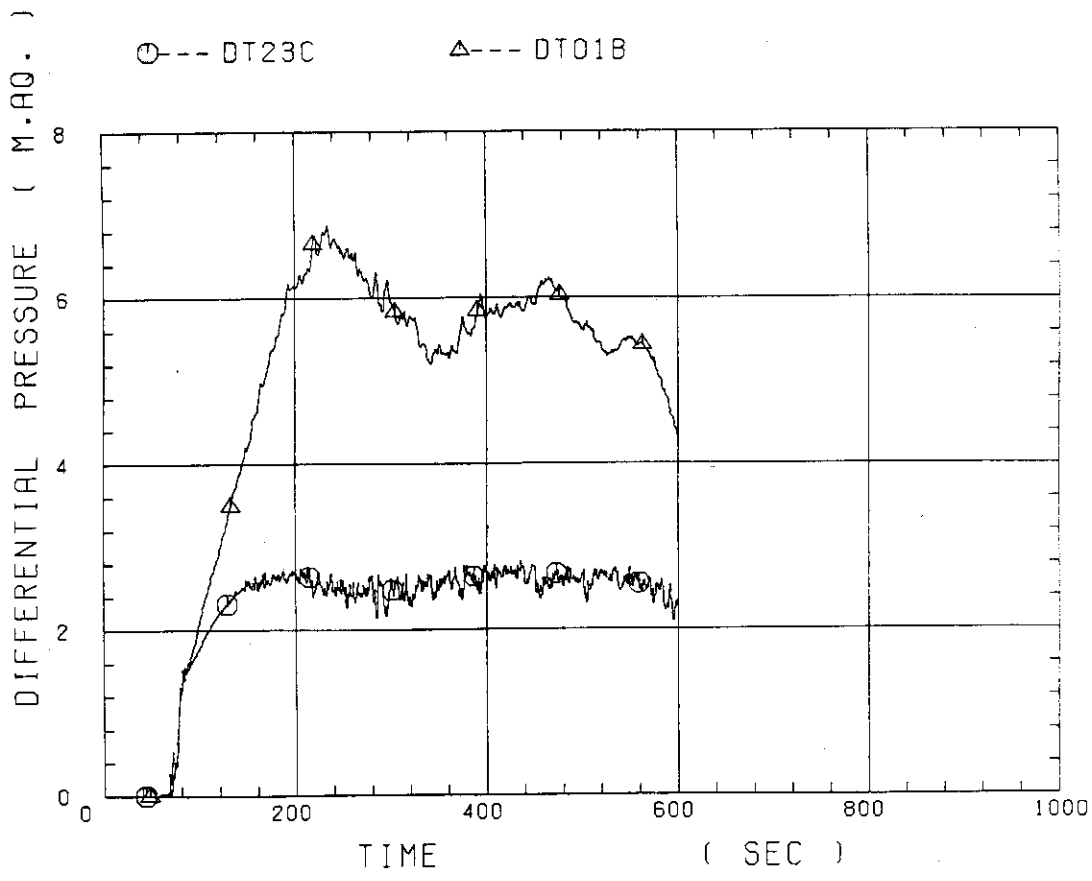

Fig. B-27 Differential pressure through intact and broken loops

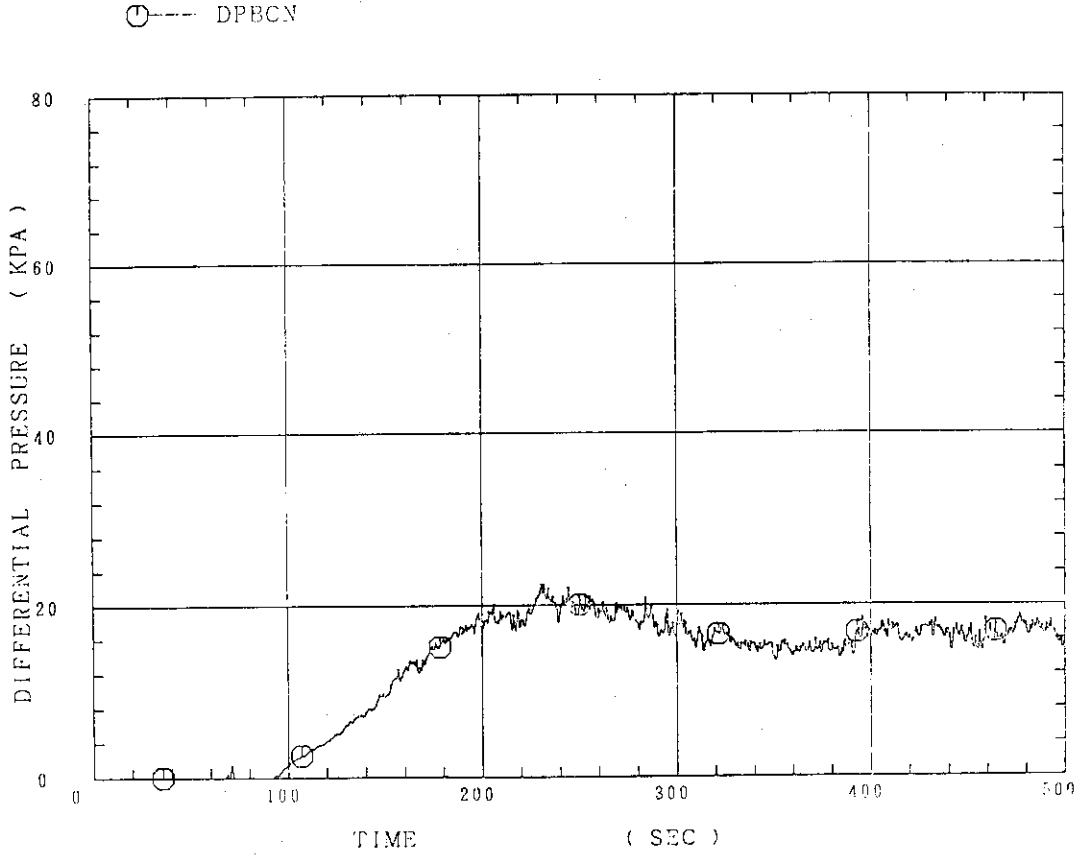

Fig. B-28 Differential pressure through broken cold leg nozzle

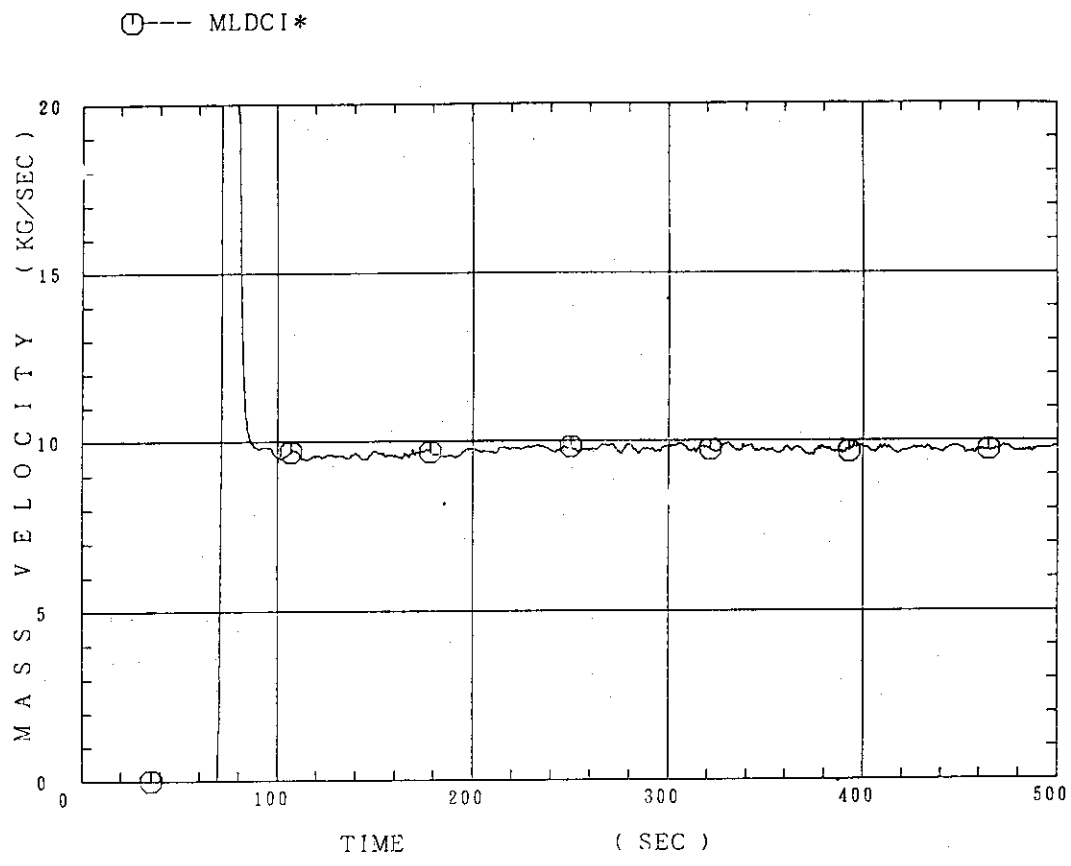

Fig. B-29 Total water mass flow rate from intact loops to downcomer

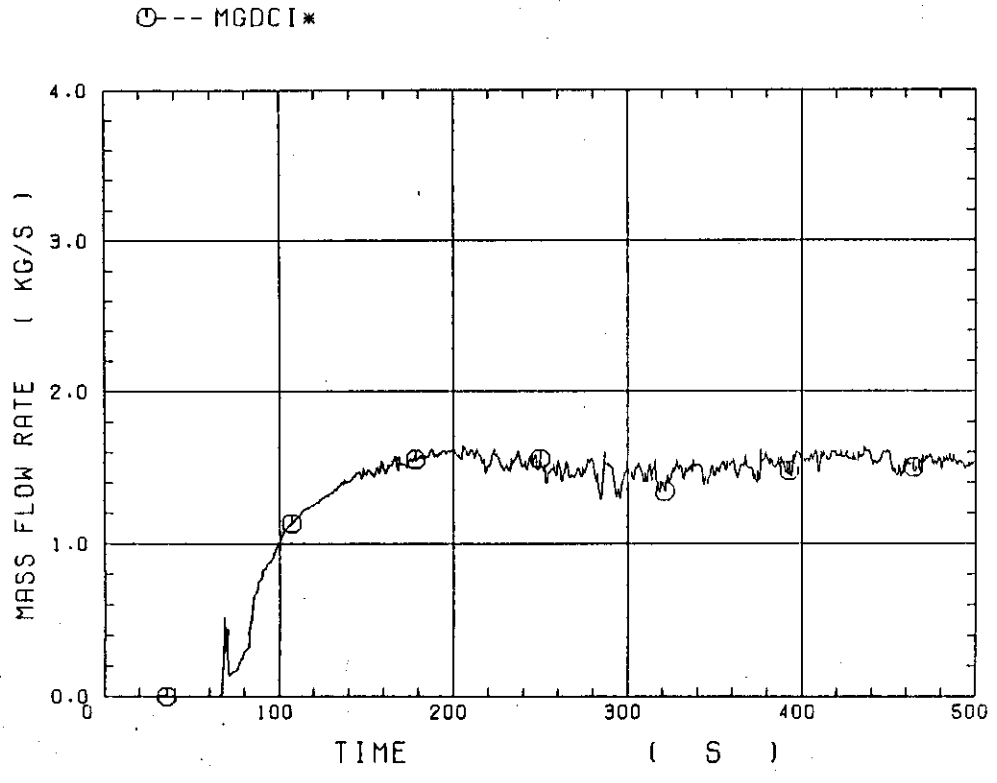

Fig. B-30 Total steam mass flow rate from intact loops to downcomer

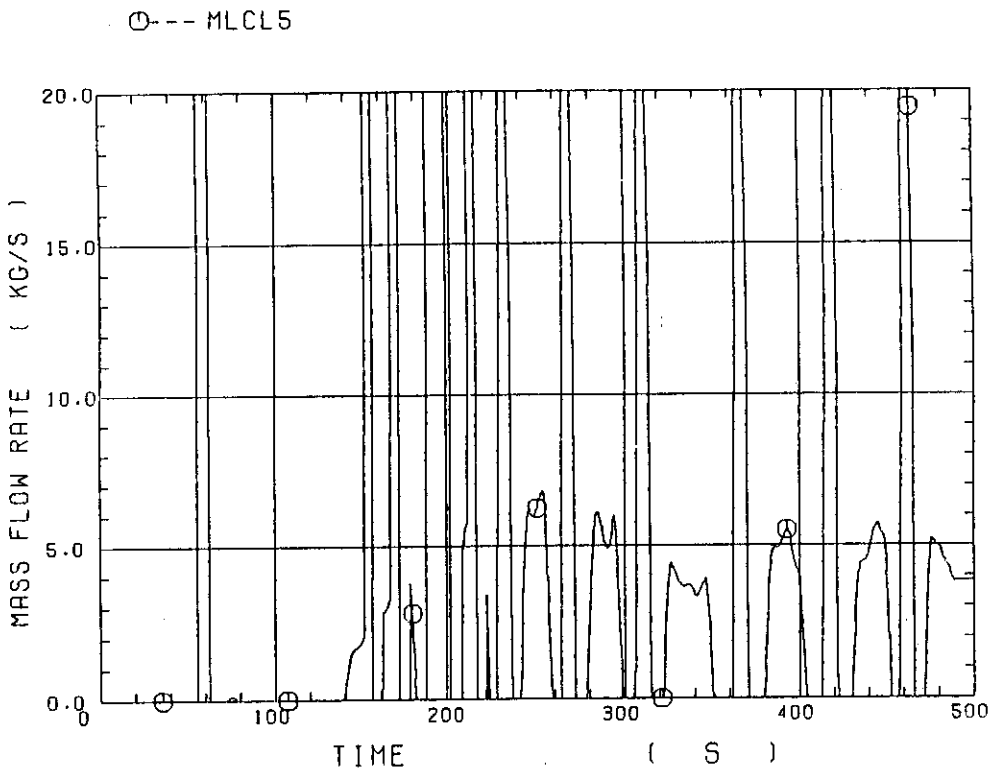

Fig. B-31 Water mass flow rate through broken cold leg nozzle

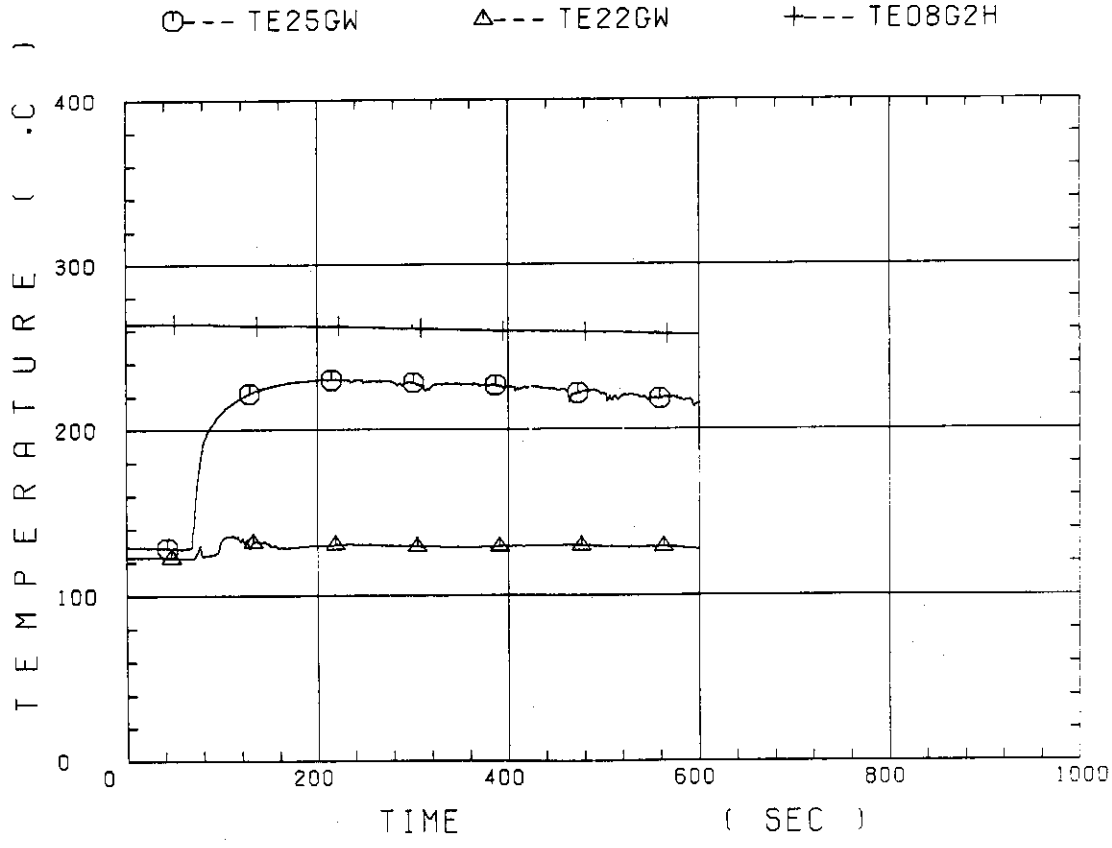

Fig. B-32 Fluid temperature in inlet plenum, outlet plenum, and secondary of steam generator 1

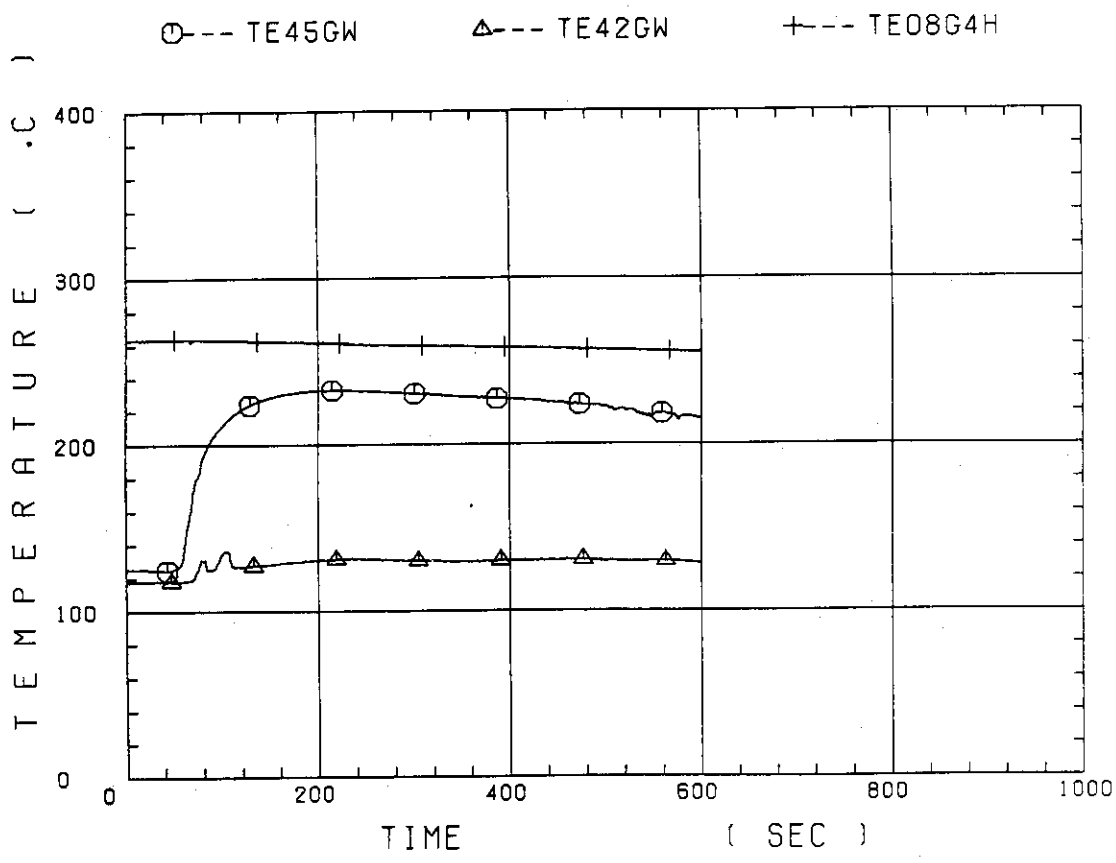

Fig. B-33 Fluid temperature in inlet plenum, outlet plenum, and secondary of steam generator 2

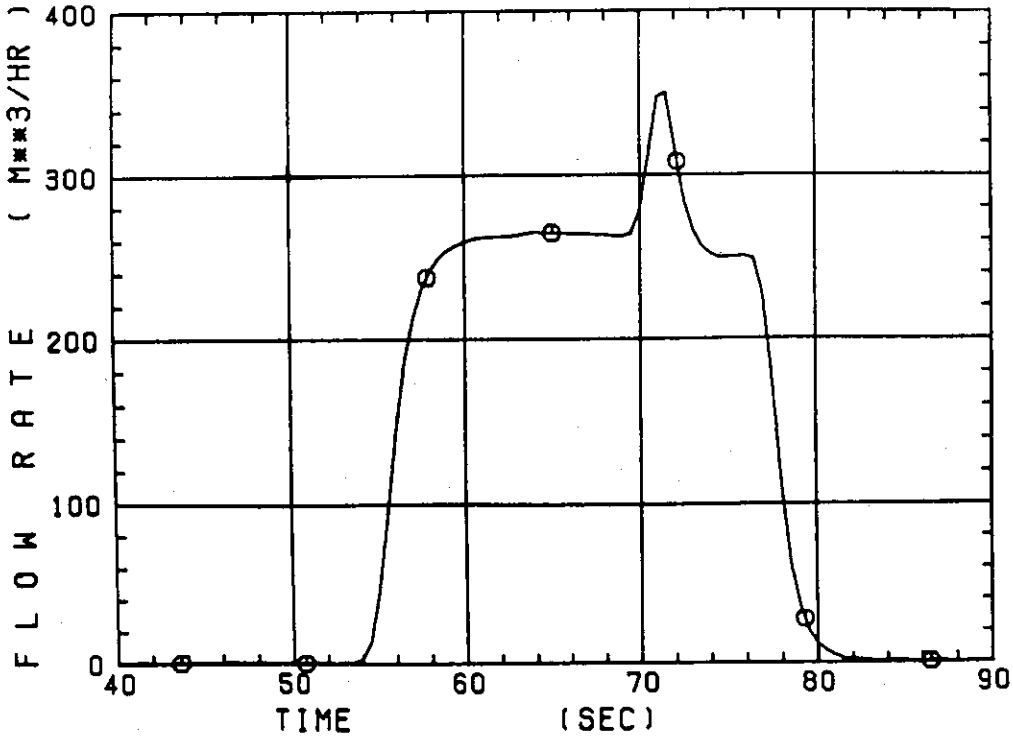

Fig. B-34 Total accumulator injection rate

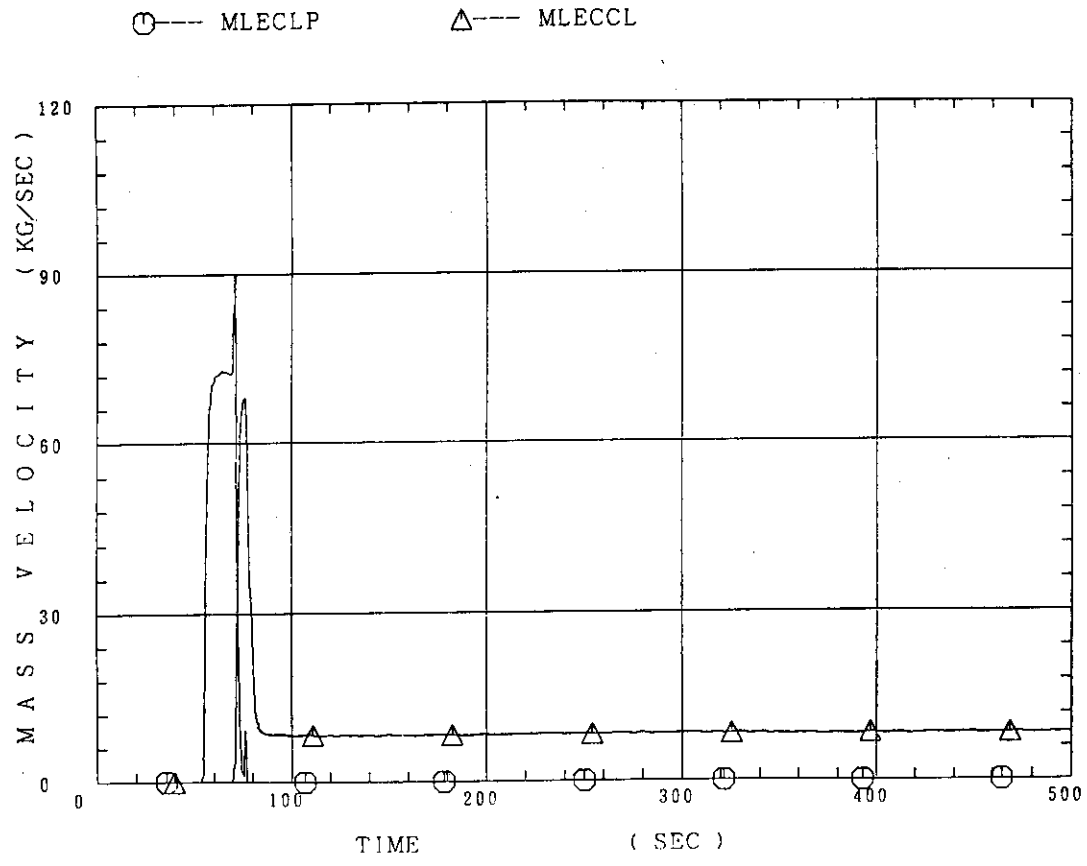

Fig. B-35 ECC water injection rates to lower plenum and to cold legs

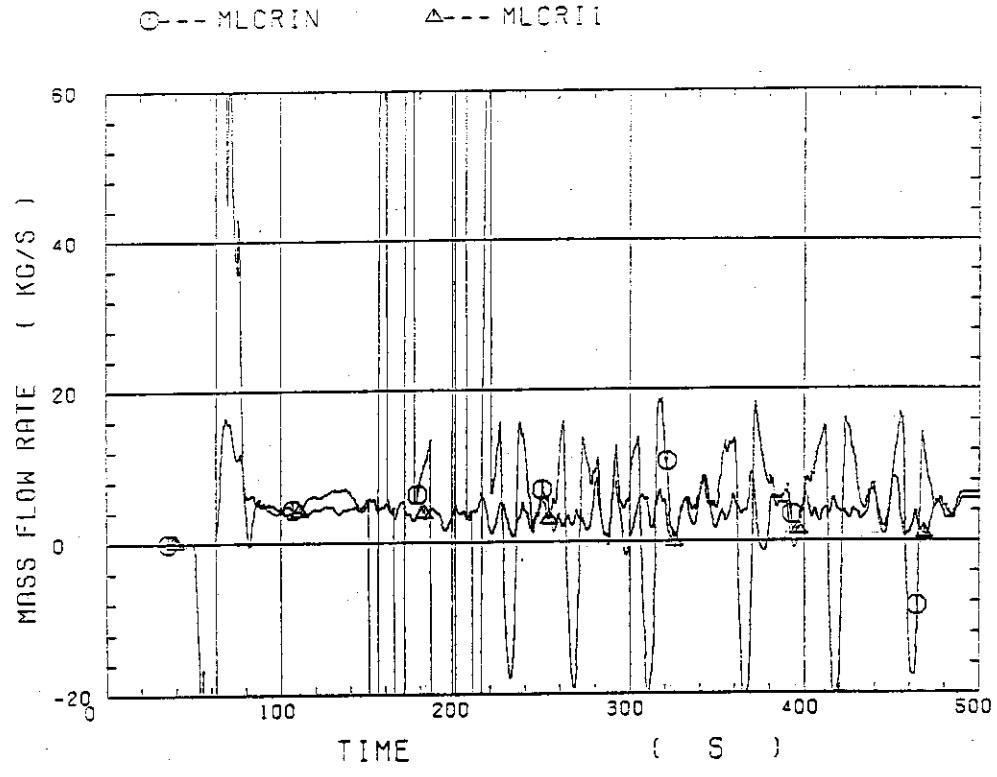

Fig. B-36 Core inlet mass flow rates estimated by mass balance downstream and upstread of core inlet

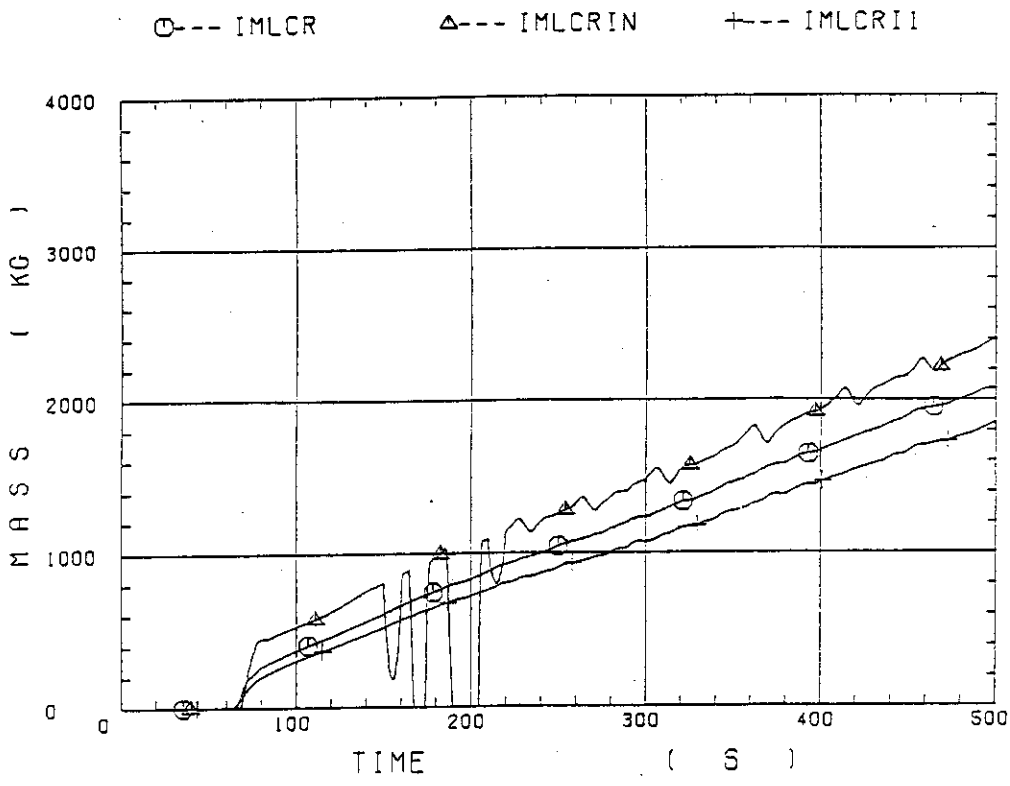

Fig. B-37 Comparison of injected mass into core among two estimation methods and evaluated mass